Gottesmann, B., Förster, H.-J., Müller, A., Kämpf, H. (2017): The concealed granite massif of Eichigt−Schönbrunn (Vogtland, Germany): Petrography, mineralogy, geochemistry and age of the Eichigt apical intrusion. - *FOG - Freiberg Online Geoscience*, *49*, pp. 1—49.

FOG

Freiberg Online Geoscience

FOG is an electronic journal registered under **ISSN 1434-7512**

2017, VOL 49

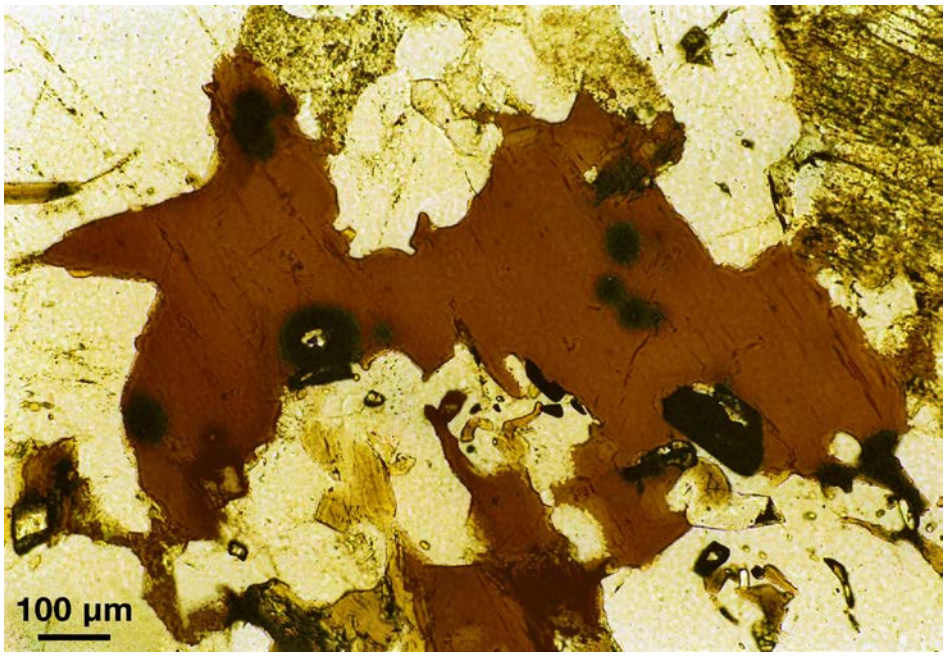

Bärbel Gottesmann, Hans-Jürgen Förster, Axel Bernd Müller, Horst Kämpf

The concealed granite massif of Eichigt–Schönbrunn (Vogtland, Germany): Petrography, mineralogy, geochemistry and age of the Eichigt apical intrusion

46 pages, 17 figures, 12 tables, 129 references

The concealed granite massif of Eichigt−Schönbrunn (Vogtland, Germany): Petrography, mineralogy, geochemistry and age of the Eichigt apical intrusion

Bärbel Gottesmann[1], Hans-Jürgen Förster[1,*], Axel Bernd Müller[2], Horst Kämpf[1]

[1] Helmholtz-Zentrum Potsdam Deutsches GeoForschungsZentrum GFZ, Telegrafenberg, 14473 Potsdam, Germany

[2] University of Oslo, Natural History Museum, P.O. Box 1172, Blindern, 0318 Oslo, Norway

*corresponding author: forhj@gfz-potsdam.de

Abstract

The Eichigt granite is one of two apical intrusions forming the concealed massif of Eichigt–Schönbrunn in the Erzgebirge–Vogtland metallogenic province of Germany. It represents a peraluminuous, medium-grained, Si-rich biotite monzo- to syenogranite of aluminuous A-type affinity and post-collisional (-orogenic) tectonic setting, which belongs to the group of medium-F, low-P Variscan granites of the Erzgebirge. Mineralogically and geochemically, the Eichigt granite shows the closest affinity to the Gottesberg subvolcanic microgranite/rhyolite complex some 25 km north-east of the massif. The granites contain phenocrysts of quartz and K-feldspar and sporadically accessory topaz and andalusite. A special feature is the presence of accessory primary fergusonite-(Y) and secondary synchysite-(Ce). Minor amounts of quartz, K-feldspar, and siderophyllite likely represent antecrysts, i.e., crystallized from a lesser silicic forerunner magma. These observations attest to the operation of magma mingling during the formation of the Eichigt granite. Calculation of Th–U–total Pb uraninite ages proves that the Eichigt and Schönbrunn granites are coeval and emplaced at about 306 ± 3 Ma (2σ), i.e., were formed during the same magmatic episode as the northwesterly Henneberg granite in Thuringia und the microgranite/rhyolith suite at Gottesberg and the Seiffen granite in the Erzgebirge–Vogtland. Geochemical data and mineralogical features do not lend support a genetical relation between the Eichigt–Schönbrunn granites and the spatially associated Sn-polymetallic veins.

Key words: A-type granite; magma mingling; biotite, synchysite-(Ce), fergusonite-(Y); Eichigt, Schönbrunn, Vogtland

1. Introduction

The Erzgebirge–Vogtland area is part of the Saxothuringian Zone of the Variscan orogen and constitutes a classical metallogenetic province in Central Europe rich in granitic rocks of various composition and ore-generating potential. At the westernmost edge of this province, the presence of a concealed granite body was assumed by indirect geological evidence since more than hundred years. First, contact-metamorphic rocks composed of andalusite- and cordierite-bearing schists (Fleckschiefer) are exposed around the village of Eichigt (Beck 1884, in Weise 1929). Second, in the adjacent Schönbrunn–Oelsnitz area, a Sn-polymetallic and fluorite ore field is situated which was suggested to be spatially related to a granite intrusion located at depth. The existence of this suspected granite intrusion, named Eichigt–Schönbrunn granite massif, was finally confirmed by drilling in 1953 (Fig. 1; Quellmalz 1959, Kämpf et al. 1991a, 1991b; Kuschka & Hahn 1996).

The massif forms two spatially separated apical intrusions at Schönbrunn and at Eichigt.The Schönbrunn granite is associated with the identically named fluorite deposit and strongly altered and chloritized, sericitized and silicified. The Eichigt granite, in contrast, is less altered and, therefore, little better suited to infer the primary magmatic signatures of the granite massif.

This paper is aimed at providing the first synopsis of the petrographical, mineralogical, and petrochemical characteristics of the Eichigt granite. Methods applied in this study include optical microscopy, electron-probe microanalysis (EPMA), cathodoluminescence (CL), and several physico-chemical techniques (XRF, XRD, IRS, AES, ICP-MS).

2. Geological setting and sampling

The granite massif of Eichigt–Schönbrunn in the Vogtland region of Germany is situated at the north-western edge of the Bohemian Massif in the Saxothuringian Zone of the Central European Variscides (Fig. 1). The Vogtland region is built up of Ordovician, Devonian, and Lower Carboniferous slates and volcanic rocks, which are intruded by granites in the late Carboniferous.

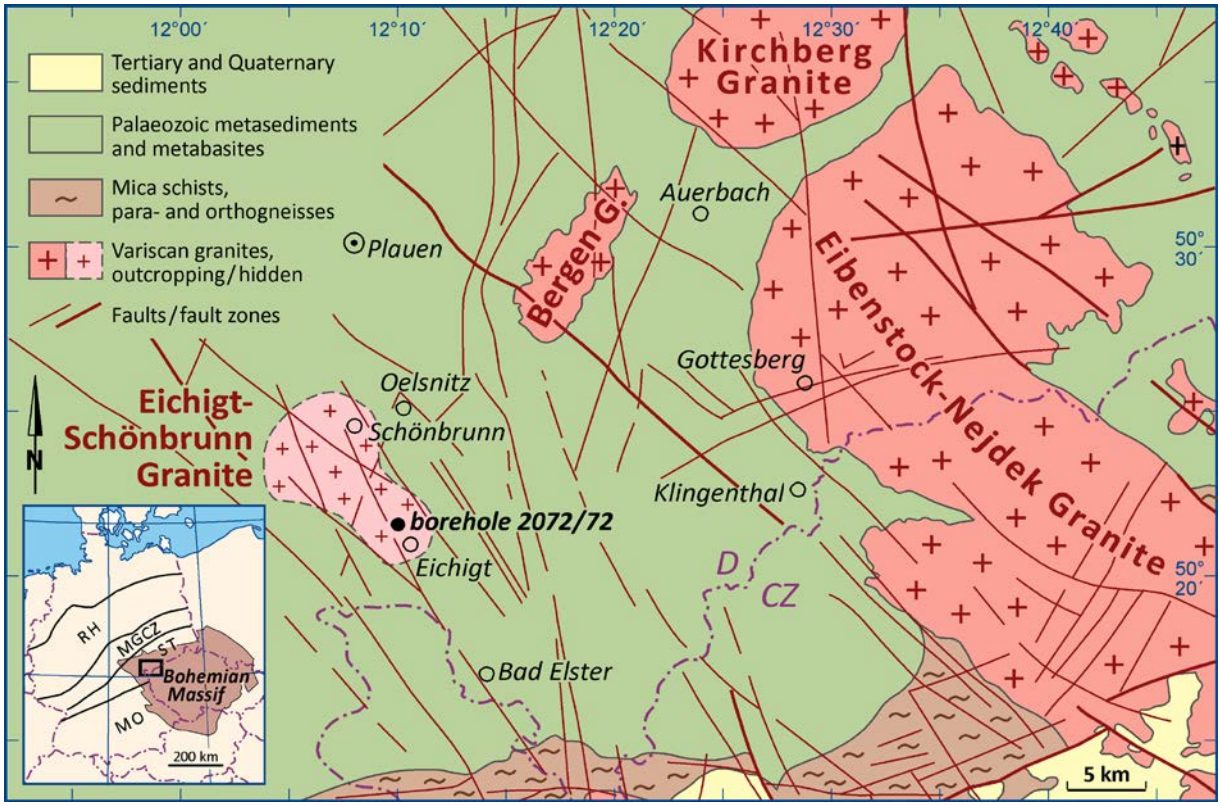

Fig. 1: Geological sketch map showing the location, size, and shape of the Eichigt–Schönbrunn granite massif in the western Vogtland of Germany within the Central European Variscides (modified after Baumann et al. 1982, Dudek 1987, Weise et al. 2001). RH – Rhenohercynian Zone, MGCZ – Mid-German Crystalline Zone, ST − Saxo-Thuringian Zone, MO – Moldanubian Zone.

Gravimetric studies (Grosse et al. 1961) and geological-mineralogical studies of borehole material (Schützel & Hösel 1962, Kämpf et al. 1991b) revealed that the NW–SE trending Eichigt–Schönbrunn granite massif has an extension of about 7.5 km (at sea level) and that its surface is split into two apical intrusions, namely, the Schönbrunn body in the NW and the Eichigt body in the SE, with a depression in between. The Eichigt and Schönbrunn apical intrusions are located close to the surface. The apex of the Schönbrunn intrusion was exposed by drilling at 380 m below surface, corresponding to +136 m above sea level. The apical portion of the Eichigt granite was encountered at a depth of 312 m (corresponding to +258 m a.s.l.)

The samples of the Eichigt granite studied in this paper represent core material taken from 2072/72 borehole drilled to a depth of 504.8 m (Table 1). The drillhole is located about 2 km NW of the village Eichigt (x = ^{55} 80 561.2; y = ^{45} 11 409.0). It penetrated about 500 meters of fleckschiefer and hornfelses above the granite. Within this contact metamorphic unit two, up to 10-cm-thick aplitic dikes were encountered at depths of 462.3 m and 476.7 m, respectively. Several small pegmatitic K-feldspar-quartz veins (thicknesses < 10 cm) occurred at depth intervals 343.5 − 349.1 m and 366.0 − 367.6 m. The top of the Eichigt granite is at 496 m depth. Alltogether, 31 drillcore samples were studied, encompassing 19 granites, eight K-feldspar–quartz veins, and four aplites (Table 1).

Table 1: Location and description of samples from borehole 2072/72.
Mineral abbrevations after Whitney & Evans (2010).

Sample No	Depth (m)	Description
1	343.5−343.6	Kfs-Qz vein and younger Qz vein. Kfs fresh
2	348.0−348.1	Kfs-Qz vein. Kfs more or less fresh
3	348.2−348.4	Kfs-Qz vein. Kfs altered
4	348.5−348.8	Kfs-Qz vein. Some fresh Kfs
5	349.0−349.1	Kfs-Qz vein. Mostly fresh Kfs
6	366.0−366.1	Kfs-Qz vein and younger Fl, minor Kfs
7	366.2−366.3	Qz vein with some Kfs
8	367.5−367.6	Qz vein with some Kfs
29–31	462.3	hornfels and homogeneous fine-grained aplite
33	476.6−476.8	hornfels and aplite with sharp contact
10	497.0−497.1	granite, mg[1)], inhomogeneous, Kfs rich, with Kfs phenocrysts, reddish
11	497.2−497.3	granite, mg, weekly porph[2)]; rounded zoned Kfs phenocryst, reddish
12	498.0−498.1	granite, mg, weekly porph, rose-colored, albitized
13	498.6−498.7	granite, close to a Qz vein altered to rose-colored albitite
14	499.0−499.1	granite, mg, weekly porph, rose and grey parts
15	500.0−500.1	granite, mg, weekly porph; Qz-Bt-accessory mineral nest; And; grey
16	500.5−500.6	granite, mg, weekly porph, grey to rose parts
17	500.6−500.7	granite, mg, weekly porph, grey to rose parts
18	500.8−500.9	granite, mg, weekly porph, grey to rose parts
19	501.0−501.1	granite, mg, weekly porph; pseudomorphs, And; grey to reddish
20	501.5−501.6	granite, mg, weekly porph, rose to reddish
21	502.0−502.1	granite, mg, weekly porph; pseudomorphs; rose-colored
22	502.5−502.7	granite, mg, weekly porph; pseudomorphs; rose + reddish zone
23	503.0−503.1	granite, mg, weekly porph; pseudomorphs; rose-colored
24	503.5−503.6	granite, mg, weekly porph, rose-colored
25	504.0−504.1	granite, mg-cg[3)], weekly porph; rounded zoned Kfs phenocryst (12mm)
26	504.6−504.7	granite, mg, weekly porph, rose-colored
27	504.7−504.8	granite, mg, weekly porph, rose-colored
28	504.8	granite, mg, weekly porph; Kfs phenocryst with graphic rim

[1)] = medium-grained. [2)] = porphyritic. [3)] = coarse-grained

3. Methods

3. 1. Mineral analyses

Analyses of rock-forming minerals were performed using CAMEBAX SX-50 and SX-100 electron microprobes at the Deutsches GeoForschungsZentrum Potsdam (GFZ) operating in the wavelength-dispersive (WDS) mode at 15 kV, 10 − 20 nA, and 5 − 15 µm beam diameter. Natural and synthetic standards were used for calibration including wollastonite (Si, Ca), rutile (Ti), orthoclase (Al, K), hematite (Fe), rhodonite (Mn), periclase (Mg), albite (Na), Ba-, Rb-, Cs-feldspar (Ba, Rb, Cs), lithium fluoride (F), tugtupite (Cl), chromium oxid (Cr), and apatite (P).

Scanning electron-microprobe cathodoluminescence (SEM-CL) and backscattered electron (BSE) images of quartz were obtained from a JEOL 5900LV analytical SEM with an attached GATAN MiniCL detector at the Natural History Museum, London. The acceleration voltage and current applied were 20 kV and ~1 nA, respectively. The CL images were collected from three scans of 20 s photo speed each and a processing resolution of 1280 by 960 pixels and 256 grey levels.

The operating conditions during EPM-analysis of accessory minerals were as follows: accelerating voltage 20 kV, beam current 40 – 60 nA, and beam diameter 1 − 2 µm. To minimize surface destruction, analysis of synchysite-(Ce) was performed with a larger beam size of 10 µm. The counting times on the peak were 300 s for Pb and 200 s for Th and U, and in each case, half that time for background counts on both sides of the peak. For the REE and other elements, counting times were 60 s and 40 s on peak, respectively. Data reduction procedure, analyzing crystals, standards, analytical precision and detection limits are described in detail in Förster (1998a,b). The standardization for the determination of the uraninite Th–U–Pb_{tot} ages was routinely checked against an in-house uraninite standard (Th–U–Pb_{tot} age = 326 ± 4 Ma, 2σ) from a granite with a U–Pb monazite age of 325 ± 2 Ma (2σ). The average error for each analysis amounted to 10 Ma.

3.2 Whole-rock geochemistry

Whole-rock geochemical analyses were performed in the laboratories at Deutsches GeoForschungsZentrum GFZ, Potsdam. Samples were ground in an agate mill to <62 µm and homogenized. Major elements + V, Cr, Ni, and Zn were analyzed by X-ray fluorescence spectrometry (XRF) of fused lithium tetraborate discs on a Siemens SRS 303 AS spectrometer using a Rh tube operated at 50 kV and 45 mA. H_2O and CO_2 were determined by IR-spectrometry (LECO CH elemental analyzer) or thermal conductivity measurements (vario EL) after decomposition of the rock powder in a 1000°C oxygen stream. Analysis for fluorine was performed using ion-selective electrodes. Trace and rare earth elements (REE) + Rb, Sr,Y, Zr, Cs, Ba, Hf, Pb, Th, and U were analyzed by inductively coupled plasma-mass spectrometry (ICP-MS) on a Perkin-Elmer/SCIEX Elan 5000 ICP mass spectrometer. Details on ICP-MS sample preparation (mixed acid digestion procedure), calibration, conditions of measurement, and precision and accuracy are outlined in Dulski (2001). Analysis for Li, Ga, Nb, Mo, Cd, Sn, Sb, Ta, W, Tl, and Bi was performed by ICP-MS (Fisons/VG Plasma Quad PQ 2+) as described by Plessen et al. (1994). Beryllium and Sc were analyzed using by atomic emission spectrometry (AES).

4. Results

4.1 Petrography

The Eichigt granite is a grey to rose-colored rock with a texture varying between equigranular medium- (to coarse-) grained to fine- to medium-grained with rare phenocrysts (Figs. 2a–c; 3). The sparse phenocrysts are mainly K-feldspar (4 − 15 mm) and/or quartz (3 − 8 mm); plagioclase is subordinate. The matrix (on average ~1 mm in grain size) is predominantly composed of K-feldspar, quartz, plagioclase, biotite, and white mica. Common accessory minerals are apatite, zircon, monazite-(Ce), xenotime-(Y), uraninite, thorite, and opaque minerals. Topaz and andalusite occur sporadically.

The modal composition of the virtually unaltered Eichigt granite determined by point counting is given in Table 2. It classifies as biotite monzo- to syenogranite according to the classification of Le Bas & Streckeisen (1991). The granite occasionally experienced minor alteration. Chlorite, white mica, secondary quartz, albite, carbonate, fluorite, and hematite are the main alteration minerals. The modal composition of granite samples with different degrees of alteration determined by X-ray diffraction (XRD) analysis is provided in Table 3. Tourmaline identified by XRD was not found in the thin sections. In some places the granite is weakly deformed showing cataclastic feldspar, micro cracks in quartz, kink bands in mica (Fig. 4a) or mortar zones (Fig. 4b). The details of the rock-forming minerals from the Eichigt granite concerning their shape, their relations with one another and their generations in the course of the granite crystallization are briefly described in Table 4.

Table 2: Modal composition (vol%) of the fresh Eichigt granite determined by point counting (Herrmann 1967)

Quartz	34
K-feldspar	29
Perthitic albite in Kfs	5
Plagioclase 1	17
Plagioclase 2*	6
Biotite	5
White mica	3
Accessory minerals	1

* = clear albitic rims and albitic overgrowths on plagioclase 1 and newly grown albite grains

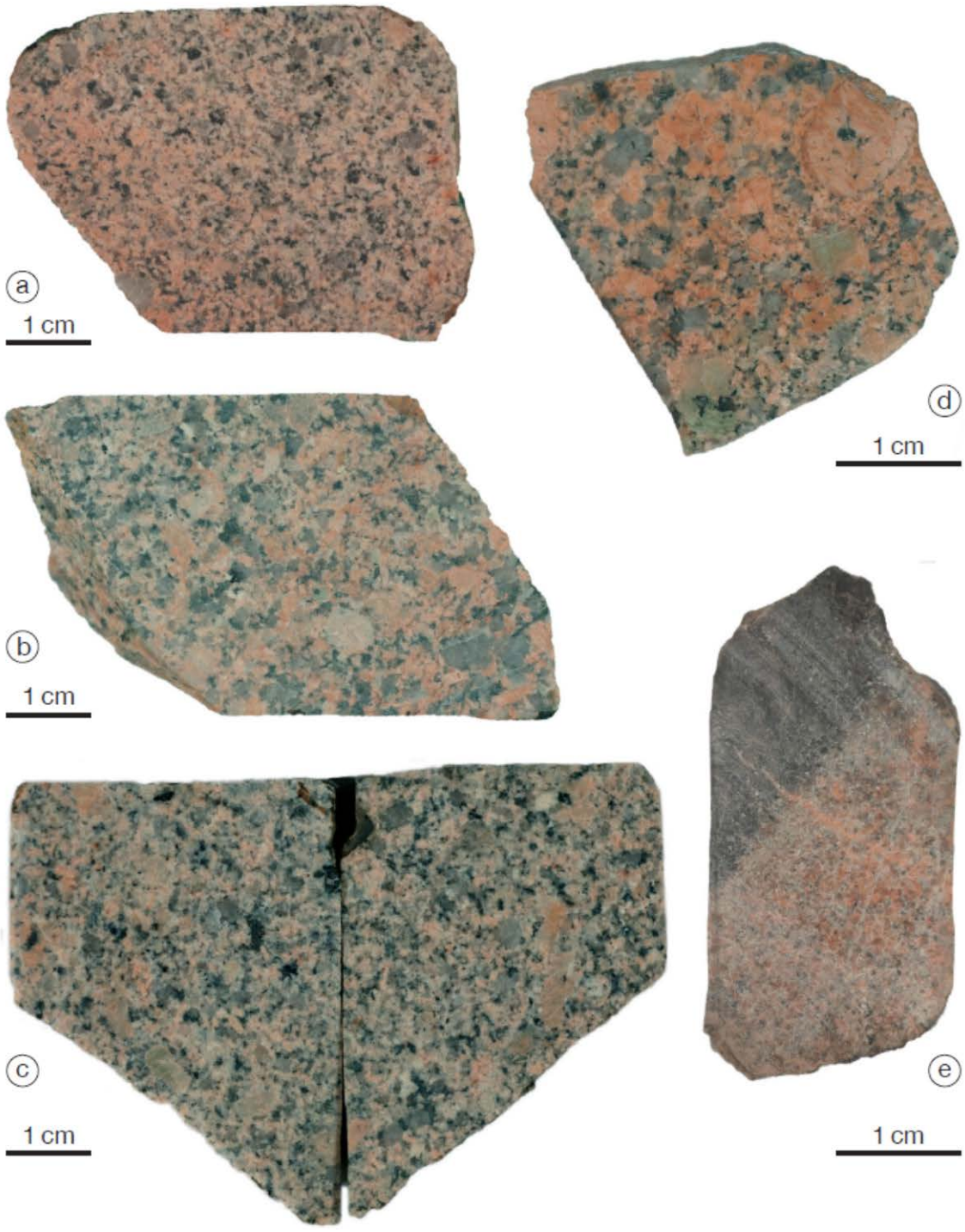

Fig 2: Hand specimens of the Eichigt granite. (a) Common equigranular medium-grained appearance (sample 23). (b) Local transition to a weakly porphyritic, coarse-grained texture (sample 25). (c) Euhedral tabular K-feldspar phenocryst (right part). − Sample 18. (d) Part of a striking rounded K-feldspar phenocryst (Kfs-A_1; top right). − Sample 11. (e) Fine-grained aplite showing sharp contact with the wall rock. − Sample 33.

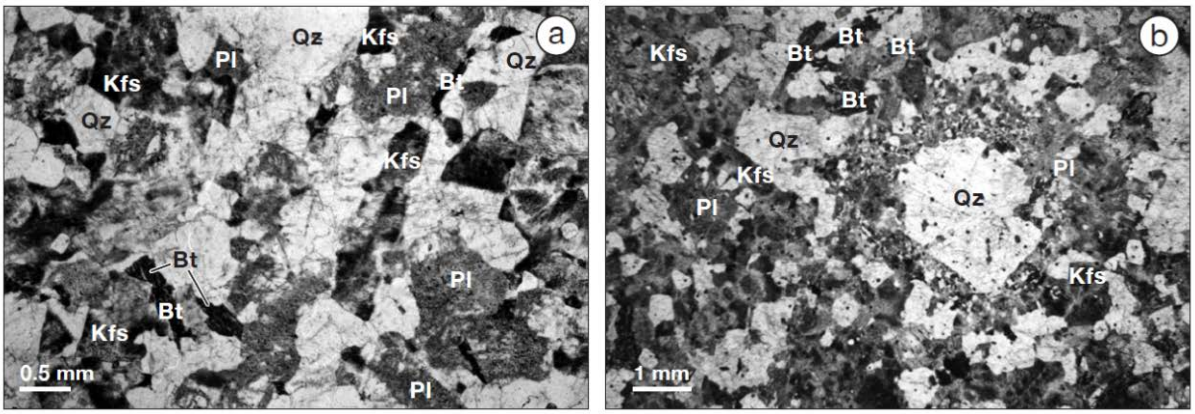

Fig. 3: Microstructure of the Eichigt granite (plain-polarized light). (a) Normal equigranular medium-grained appearance (thin section 15 A). (b) Weakly porphyritic (fine- to) medium-grained granite with a subhedral quartz phenocryst (Qz-A) surrounded by a fine-grained Qz-Kfs rim (thin section 11 B).

Table 3: Modal mineralogy (wt%) of granite samples from borehole 2072/72 determined by XRD

Sample No.	15	19	21	22	12
Quartz	33	35	30	31	35
Orthoclase	3	4	5	4	1
Microcline maximum	28	23	24	23	2
Oligoclase	14				
Albite	12	29	27	30	56
Muscovite $2M_1$ / Illite	6	5	10	10	3
Chlorite		0.7	1.0	0.9	1.2
Topaz	2.3	1.8	1.1	0.8	
Fluorapatite					0.5
Hematite			0.6	0.4	0.6
Tourmaline (Schorl)	1.2	1.2	1.3		0.9

The aplites in the hanging hornfels are grey to rose-colored, uneven-grained rocks (Figs. 2e, 4c, 4d) consisting of quartz, albite, muscovite, some K-feldspar, accessory apatite (Fig. 4c) and radioactive accessories plus traces of fluorite and secondary carbonate. They are fine-grained, with grain sizes typically varying between ~ 0.2 mm and ~ 1 mm (locally 3 mm). The contact with the wall-rock is sharp (Figs. 2e, 4d). Occasionally, the contact is accompanied by mm-thick medium-grained zones showing unidirectional solidification texture (UST sensu stricto; Shannon et al. 1982) made up of muscovite flakes and quartz columns, which are oriented perpendicular to the contact (Fig. 4d). This texture suggests that the grains formed at a mineral-liquid interface during the inward crystallization of the aplite.

Table 4: Stages of mineral formation in the Eichigt granite

Stage	progenitor magma	early magmatic	magmatic	late-magmatic	post-magmatic	hydrothermal
biotite	Bt-A, forming clusters; antecrysts	Bt-B, inclusions in Qz; core of Bt-C; richer in (Fe+Ti)	Bt-C matrix, main quantity, richer in ^{VI}Al		(kink bands)	
plagioclase	Pl-A ?	eu- to subhedral phenocrysts	sub- to anhedral matrix		albite (cataclasis)	
K-feldspar	rounded Kfs-A_1 phenocrysts; richer in Ba; antecrysts	euhedral Kfs-A_2 true phenocrysts	anhedral or granophyric Kfs-B matrix		(cataclasis)	
quartz	Qz-A_1 antecrysts	Qz-A_2 true eu- to subhedral phenocrysts	Qz-B anhedral or granophyric matrix	Qz-C corrosive	fracturing micro-brecciation	
white mica				WM-A, rich in Al + Na	WM-B, rich in F	WM-C, rich in Si, Fe, Mg and Rb; F-free
andalusite						
topaz						
chlorite						
fluorite						
carbonate						

The small pegmatite veins are composed of anhedral coarse, rose K-feldspar (grain size up to 1 cm), coarse massive quartz and minor greenish-white plagioclase in small nests. One sample contained aggregates (up to 4 mm in diameter) and single grains of pyrite (≤ 1 mm in size). The pegmatite veins also contain angular fragments of the hornfels wall rock.

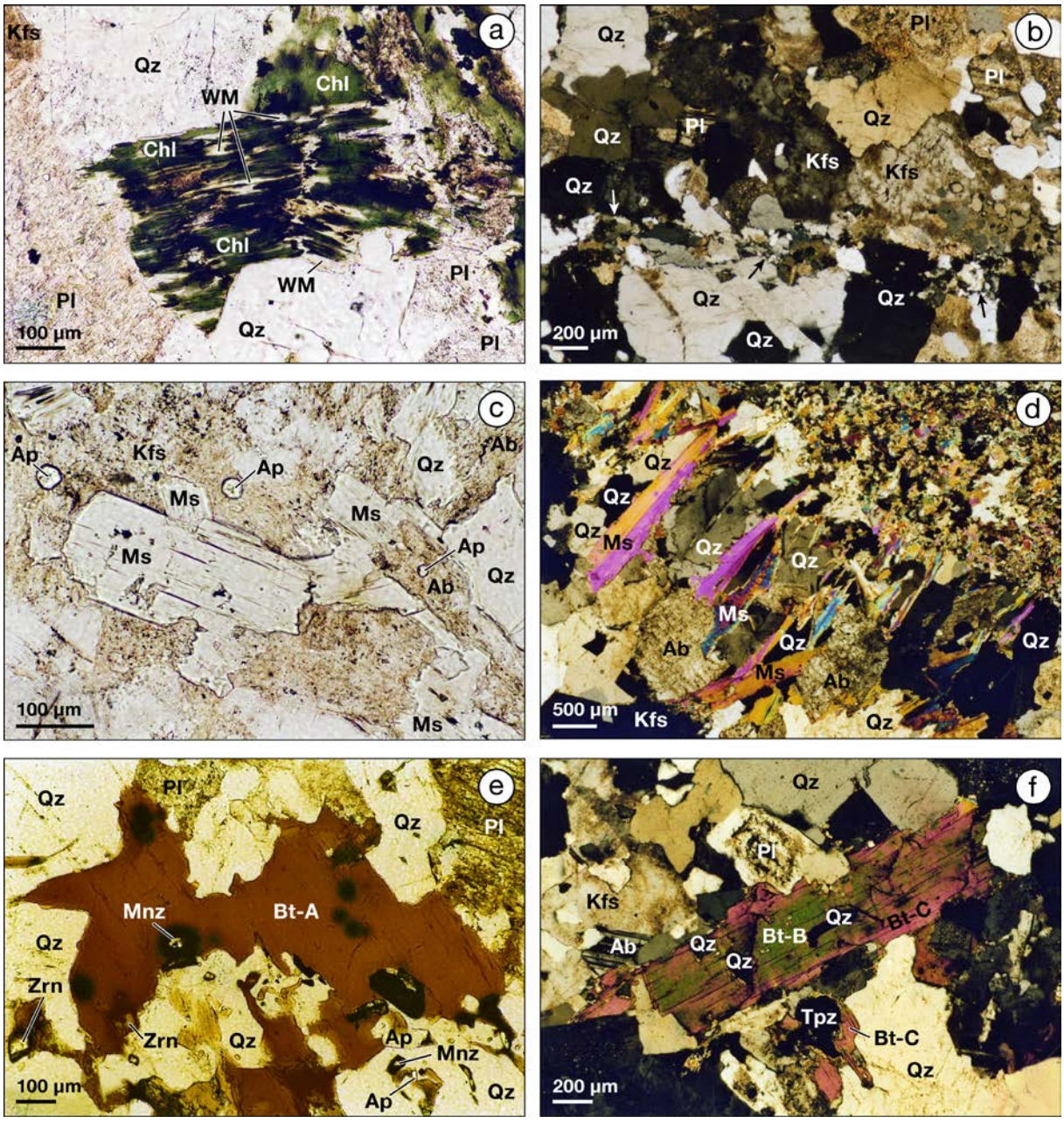

Fig. 4: Microstructures of the Eichigt granite and aplite. (a) A kink band in totally altered biotite in granite caused by weak cataclasis (WM = white mica). − Plane-polarized light; thin section 11B. (b) A narrow nearly horizontal mortar zone (lower part, 3 arrows) in the granite. − Crossed polars; thin section 22. (c) Subhedral Ms plates within the equigranular fine-grained aplite also containing Ab, Kfs, Qz, and Ap. – Plane-polarized light; thin section 30. (d) Unidirectional solidification texture shown by Ms flakes and Qz columns at the contact between aplite dike (bottom left and centre) and wall rock (top right). − Crossed polars; thin section 33. (e) Bt-A−Qz cluster rich in accessoric minerals. The anhedral Bt-A contains several radioactive haloes. − Plane-polarized light; thin section 15A. (f) Zoned granite biotite with core of Bt-B (green) surrounded by Bt-C (red) containing three Qz inclusions (black). The black grain intergrown with Bt-C represents an anhedral topaz (Tpz). − Crossed polars; thin section 15A.

4.2 Mineralogy and mineral compositions

4.2.1 Biotite

The composition of the three biotite populations A, B, and C is given in Table 5. The contents of P (0 – 0.04 wt% P_2O_5), Cr (0 – 0.1 Cr_2O_3), and Ba (0 – 0.09 BaO) are negligible. All varieties classify as siderophyllite (Foster 1960, Rieder et al. 1998, Tischendorf et al. 2004, 2007). Chemically, the differences between the three mica varieties are small, but distinct. The (Fe_{tot} + Ti) vs. $^{[6]}$Al plot (Fig. 5) shows an evolutionary trend from presumably early magmatically crystallized, relative (Fe + Ti)-rich Bt-B to the apparently later grown Bt-C, which is richer in octahedral Al. Bt-A takes an intermediate position with respect to the concentrations of (Fe + Ti) and $^{[6]}$Al.

Table 5: Representative results of EPM analyses (wt%) of biotite

	Biotite A	Biotite B		Biotite C		Average (1σ)
sample No.	15	11B	15	12; albitized	15	
point No.	Bi1/5	Bi2/1	Bi4/11	Bi2/2	Bi3/1	n = 42
SiO_2	36.4	34.8	35.4	36.6	36.3	36.2 (0.60)
TiO_2	1.78	1.75	2.31	1.91	1.43	2.02 (0.50)
Al_2O_3	20.6	19.4	19.6	21.1	20.4	20.4 (0.50)
FeO[a]	25.4	27.8	26.8	24.5	25.8	26.1 (0.71)
MnO	0.49	0.55	0.56	0.50	0.47	0.50 (0.05)
MgO	1.62	1.55	1.50	1.45	1.63	1.57 (0.16)
CaO	0.00	0.00	0.00	0.02	0.00	0.00 (0.01)
Li_2O[b]	0.43	0.45	0.46	0.48	0.43	0.44 (0.03)
Na_2O	0.21	0.23	0.19	0.25	0.21	0.21 (0.03)
K_2O	9.36	9.15	9.13	9.33	9.35	9.23 (0.09)
Rb_2O	0.25	0.08	0.24	0.12	0.28	0.23 (0.06)
Cs_2O	0.02	0.03	0.02	0.02	0.06	0.03 (0.03)
H_2O[c]	3.22	2.42	2.95	2.29	3.32	3.05 (0.28)
F	1.28	2.76	1.75	3.25	1.07	1.64 (0.58)
Cl	0.20	0.22	0.18	0.22	0.12	0.18 (0.02)
Sum	101.18	101.27	101.14	101.99	100.82	
O=(F+Cl)	0.58	1.21	0.78	1.43	0.48	
Total	100.59	100.05	100.37	100.56	100.34	
mgli	0.053	0.040	0.03	0.019	0.056	0.045 (0.029)
feal	1.107	1.427	1.357	1.007	1.122	1.203 (0.132)
Fe/(Fe+Mg)	0.898	0.910	0.909	0.905	0.899	0.903 (0.008)

[a] = total Fe as FeO; [b] = calculated according to equation 2 for micas of the low Mg–Li group in Tischendorf et al. (1999a); [c] = calculated assuming that the (F,Cl,OH,O) site is filled.

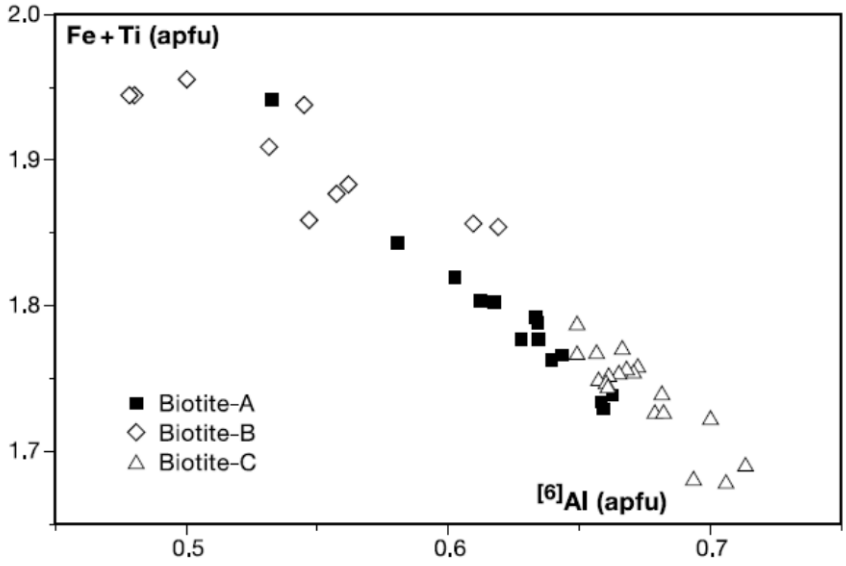

Fig. 5: (Fe+Ti) vs. $^{[6]}$Al diagram of the three siderophyllite varieties from the Eichigt granite.

The average composition of siderophyllite from Eichigt is consistent with the composition of biotite from biotite+muscovite granites (Nachit et al. 1985). In the discrimination diagrams for biotite from anorogenic extensional-related alkaline rocks (A field), metaluminous calc-alkaline I-type subduction-related suites (C field), and peraluminous S-type granites (P field) of Abdel-Rahman. (1994), all siderophyllite varieties plot in theP field. After Dahlquist et al. (2010), biotite from ferroan (A-type) granitoids has $Fe^{2+}/(Fe^{2+}+ Mg) > 0.8$ and an elevated F content, signatures consistent with those of the Eichigt-granite siderophyllite (Table 5).

Frequently, biotite is altered to an intensely green chlorite, which itself is replaced by hydrothermal white mica (Figs. 4a; 6a).

4.2.2 White mica

Compositional data for white micas from the Eichigt granite and aplite are summarized in Table 6 and illustrated in Fig. 7.

Chemically, late-magmatic WM-A is characterized by high Al_{tot}, relatively high Na, and low contents of Si, Fe, Mg, Rb, and F. Relative to the other WM from Eichigt, this population is closest to ideal muscovite. Compositionally, WM-A resembles the magmatically grown white micas from the aplitic dikes characterized by Na/(Na + K) = 0.09 and K/Rb = 85 (*cf.* Table 6).

Table 6: Representative results of EPM analyses (wt%) of white micas (WM)

Rock	Granite									Aplite	
Stage	late-magmatic WM-A			early post-magmatic WM-B			hydrothermal WM-C			magmatic	
Sample No.	15	Average	1σ	15	Average	1σ	11 B	Average	1σ	Average	1σ
Point No.	Mu4/3	n = 6		Mu3/1	n = 12		Mu4/3	n = 22		n = 15	
SiO_2	47.3	47.1	0.19	47.5	47.6	0.96	48.4	48.9	0.37	47.4	0.46
TiO_2	0.01	0.01	0.01	0.05	0.14	0.11	0.69	0.30	0.13	0.02	0.01
Al_2O_3	35.0	36.8	1.65	30.0	30.5	0.77	28.5	28.5	0.65	34.2	0.83
FeO[a]	2.54	1.55	1.01	6.16	5.67	0.98	6.54	6.50	0.42	3.08	0.41
MnO	0.07	0.04	0.02	0.14	0.11	0.03	0.04	0.09	0.04	0.03	0.02
MgO	0.22	0.15	0.09	0.99	0.67	0.20	0.96	1.18	0.26	0.22	0.25
CaO	0.00	0.00	0.01	0.01	0.00	0.01	0.01	0.01	0.01	0.00	0.01
Na_2O	0.75	0.80	0.13	0.44	0.37	0.06	0.09	0.07	0.02	0.61	0.10
K_2O	10.2	10.1	0.12	10.3	10.3	0.07	10.3	10.4	0.21	10.3	0.11
Rb_2O	0.11	0.05	0.05	0.18	0.19	0.02	0.31	0.26	0.06	0.11	0.03
Cs_2O	0.01	0.01	0.01	0.00	0.00	0.01	0.00	0.01	0.01	0.01	0.01
H_2O[b]	4.17	4.46	0.18	3.46	3.61	0.20	4.41	4.43	0.03	4.47	0.08
F	0.77	0.26	0.29	2.00	1.69	0.42	0.00	0.01	0.02	0.09	0.14
Cl	0.00	0.00	0.00	0.02	0.02	0.02	0.01	0.00	0.00	0.00	0.01
Sum	101.14			101.30			100.23			100.61	
O=(F+Cl)	0.32			0.85			0.02			0.04	
Total	100.8			100.4			100.2			100.6	
K/Rb	85	182		52	49		30	36		85	
Na/(Na+K)	0.10	0.11		0.06	0.05		0.01	0.01		0.09	
mgli	0.02	0.02		0.10	0.07		0.10	0.12		0.02	
feal	–1.81	–1.83		–1.27	–1.33		–1.16	–1.19		–1.66	

[a] = total Fe as FeO; [b] = calculated assuming that the (F, Cl, OH, O) site is filled.

Relative to WM-A, post-magmatic WM-B (Figs. 6b-c) is lower in Al_{tot} and Na, but higher in Si, Fe, Mg, and Rb, and most rich in fluorine (0.8 – 2.5 wt% F, corresponding to 0.17 – 0.54 *apfu F*).

Hydrothermal WM-C is lowest in Al_{tot} and Na and highest in Si, Fe, Mg, and Rb. This mica is almost devoid of F. The *mgli-feal* evolution of WM-A through WM-B to WM-C (Table 6) implies continuously increasing (Fe + Mg) contents and decreasing Al in favor of Si. The trend of decreasing Na and Al and concomitantly increasing Fe, Mg, and Si in the evolutionary history of white micas was also recognized by Miller et al. (1981), Monier et al. (1984), Speer (1984), Konings et al. (1988), Kontak (1991), Dempster et al. (1994) Du Bray (1994), Gomes & Neiva (2000), Dahlquist et al. (2005).

Their mean K/Rb ratio decreases from 182 in late-magmatic micas to 49 (post-magmatic) down to 36 in hydrothermally formed WM (Table 6). This trend in the temporal evolution of the K/Rb ratio in white micas is in line with the results of previous studies (Černý & Burt 1984, Jolliff et al. 1987, Alfonso et al. 2003). Deer et al. (2003) – based on data by Monier et al. (1984) – suggested to use the ratio Na/(Na + K) to discriminate between genetically different white micas in granites. They observed Na/(Na + K) ratios between 0.12 and 0.06 in magmatic muscovite, 0.07 – 0.01 in late- to post-

magmatic muscovite, and <0.04 in hydrothermal muscovite. This genetical subdivision well corresponds with the mean Na/(Na + K) ratios of WM from the Eichigt granite: WM-A – Na/(Na + K) = 0.11, WM-B – 0.05, WM-C – 0.01, respectively.

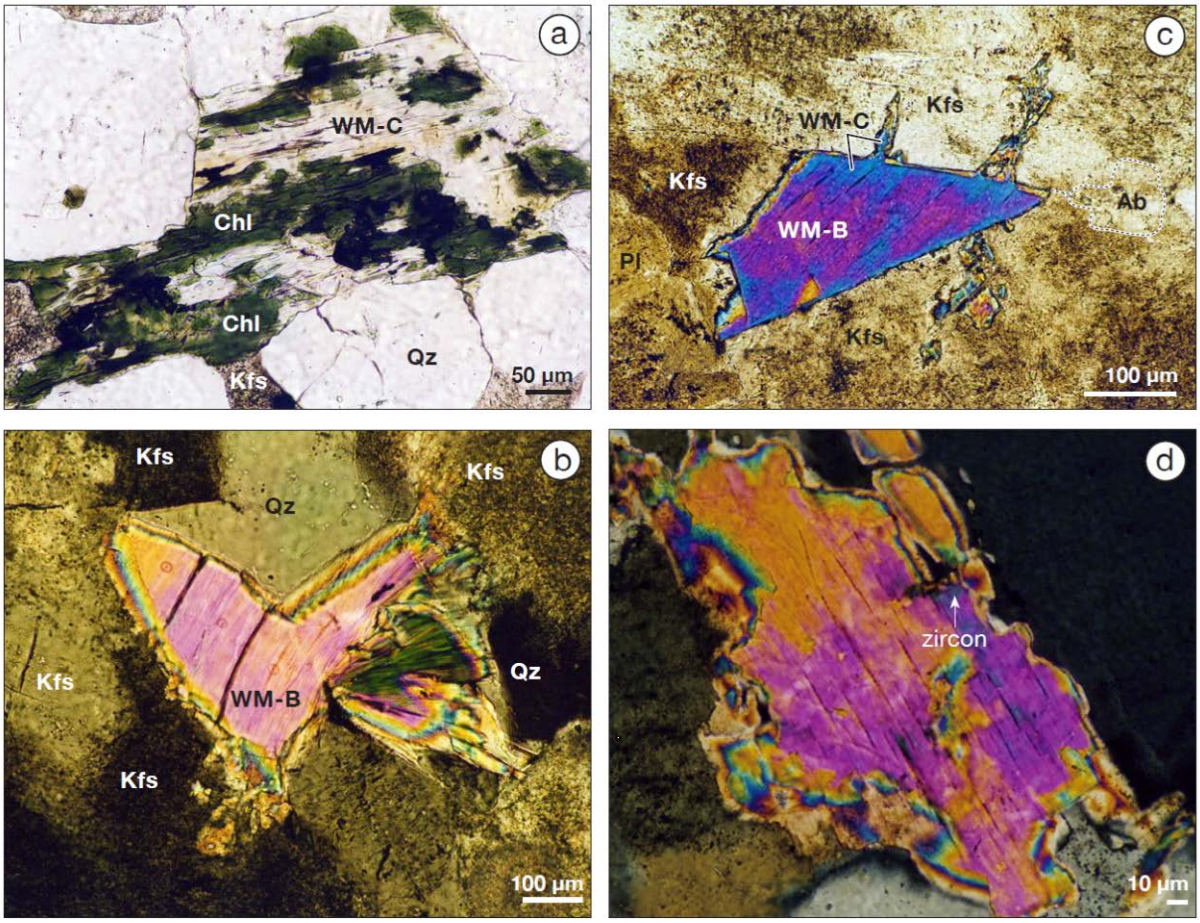

Fig. 6: (a) Totally altered biotite now consisting of white mica WM-C and intensely green chlorite with opaque minerals and accessoric leucoxene. − Plane-polarized light; thin section 11B. (b) Early post-magmatic white mica WM-B in interstice between quartz and feldspar and spherulitic white mica. − Polars partly crossed; thin section 15A. (c) Irregularly zoned white mica with WM-B core (pink) and WM-C alteration rim (blue) in the interstice between Kfs grains, growing in optical continuity into the adjacent Kfs. − Crossed polars; thin section 23. (d) Anhedral white mica strongly inhomogeneous due to alteration, replacement, and growth at changing conditions. Purple = Fe-poor, Al-rich late-magmatic core. Orange = Fe-rich, Al-poorer post-magmatic part. Yellow = Fe-rich, extremely Al-poor hydrothermal part. (see also Fig. 8 and 9). − Crossed polars; thin section 15A.

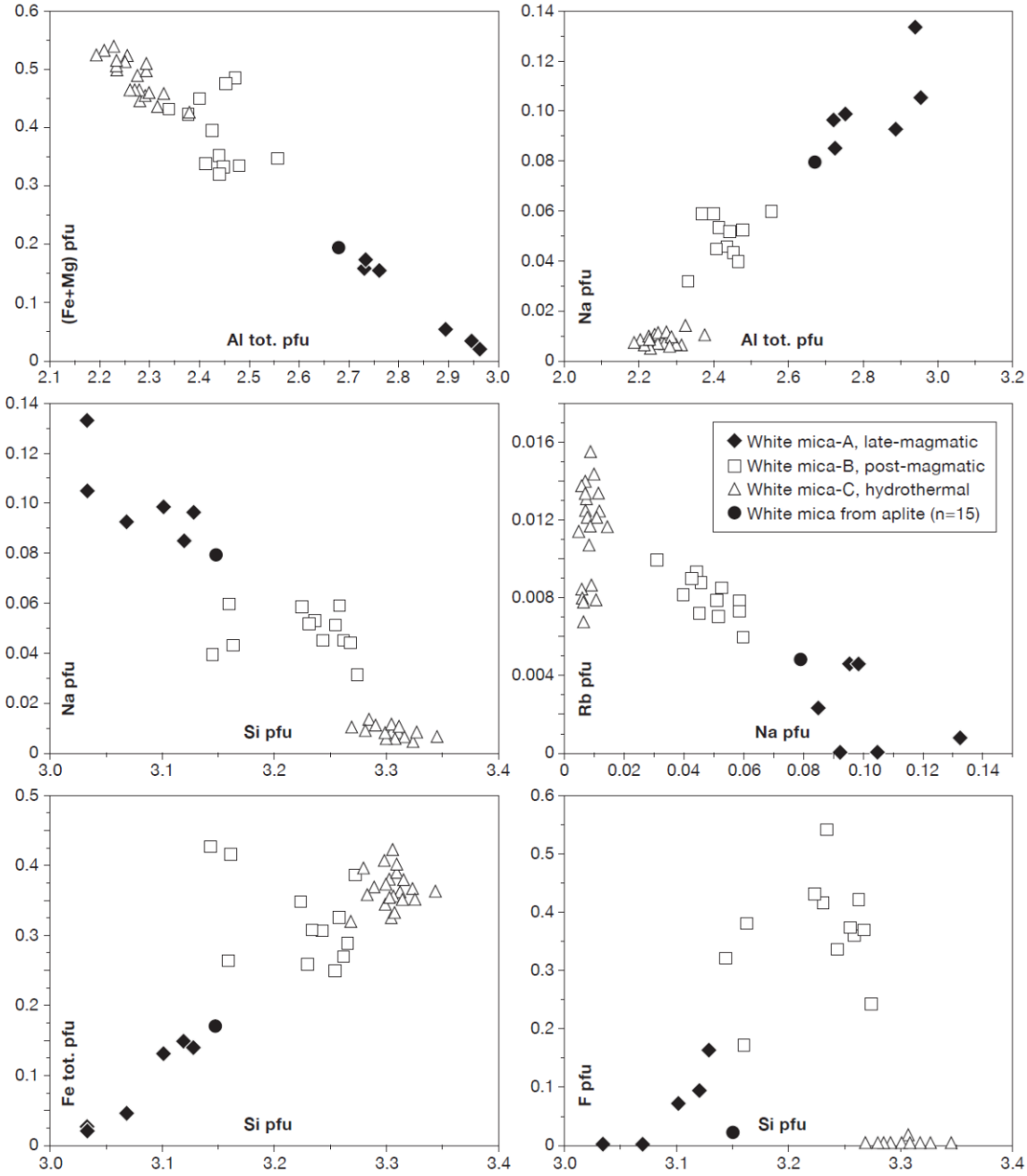

Fig. 7: Chemical characterization of white micas from the Eichigt granite and aplite in terms of (Fe+Mg), Na, Si, F, Rb, Al_{tot}, (in *apfu*).

The Ti content of white micas has been frequently used to distinguish between primary micas with high Ti and secondary micas with low Ti concentrations. This criterion does not work for the Eichigt white micas. The WM from aplites and those hosted in granitic K-feldspar and precipitated along grain boundaries, which are interpreted as late-magmatic, display low Ti (0.02% and 0.01wt% TiO_2, respectively). On the other hand, the hydrothermal WM-C originated by replacement of siderophyllite is substantially higher in Ti (~ 0.30 wt% TiO_2). We interpret this fact as result of isomorphic incorporation of Ti released from dissolution of pre-existing Ti-bearing siderophyllite into the WM structure.

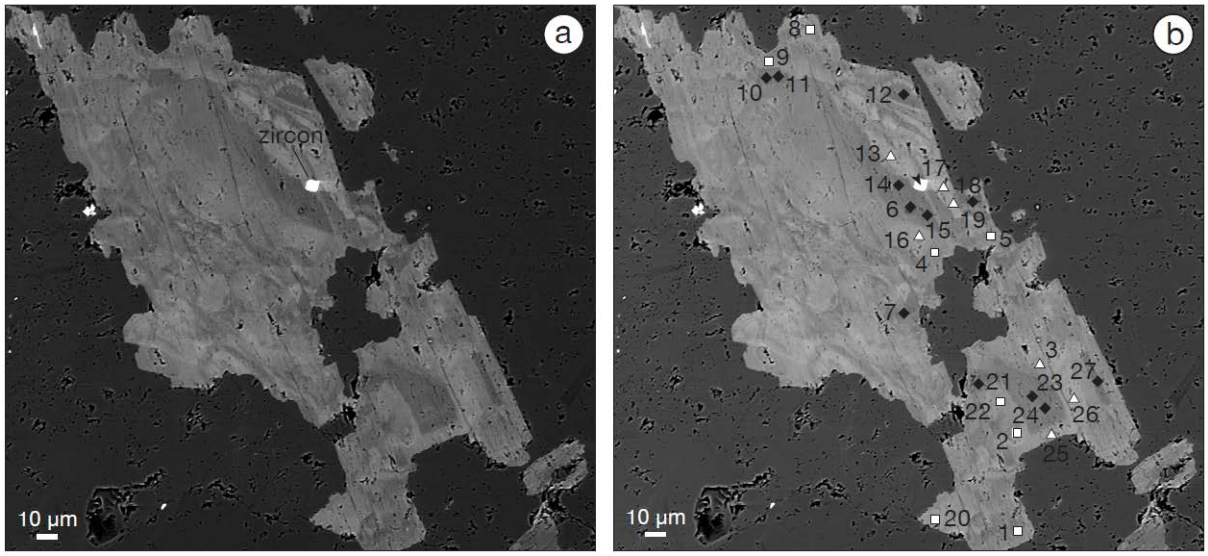

Fig. 8: (a) Back-scattered electron image of the strongly inhomogeneous white mica grain shown in Figure 6d. (a) Dark areas = relicts of the late-magmatic core (WM-A), Fe-poor and Al-rich. Bright areas = Fe-richer, Al-poorer domains developed by younger alteration, replacement or overgrowth. (b) Same as Fig. 8a with marked and numbered EPM spots (*cf.* Figure 9). Symbols as in Figure 7.

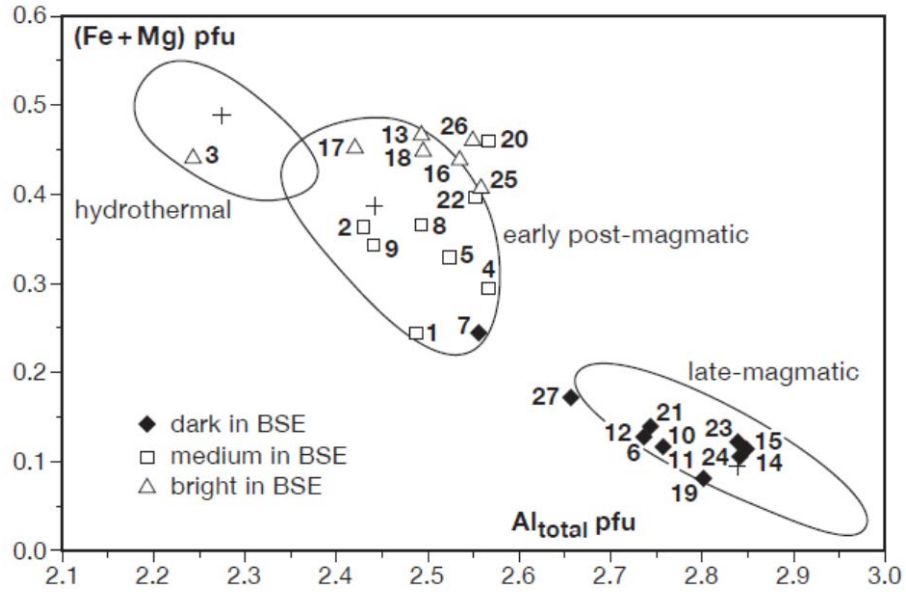

Fig. 9. (Fe+Mg) versus Al_{tot} plot reporting the results of 27 EMP spots conducted in the strongly inhomogeneous white mica grain displayed in Figures 6d and 8. Also shown are the compositional fields of late-magmatic, early post-magmatic, and hydrothermal white micas from the Eichigt granite and their respective compositional averages (plus signs).

The white mica varieties are the products of a continuously proceeding evolution. This process – also documented e.g. by Dempster et al. (1994) and Gomes & Neiva (2000) – locally gave rise to inhomogeneous grains caused by overgrowth, recrystallization, alteration, or replacement. This inhomogeneity is microscopically highlighted by undulose extinction and different birefringence

(Figs. 6c-d), strong contrasts in back-scattered electron images (BSE) (Fig. 8), and compositional heterogeneity as revealed by EPM data (Fig. 9).

4.2.3 Plagioclase

The plagioclase phenocrysts Pl-A are commonly altered to white mica forming small flakes and dense masses (sericite). Therefore, their original chemical composition could not be inferred. Likewise, most matrix plagioclase Pl-B grains are decomposed.

Matrix plagioclases grains, which were only weakly overprinted, were present only in sample 15. They classify as acid oligoclase, are poor in trace elements (Sr, Ba, Rb, P < 0.1 wt%) and show a weak chemical zoning, with 12 % anorthite and 2% orthoclase components in the core and 4 – 7% anorthite and 3% orthoclase close to the rim. Clear plagioclase patches of all other samples (n=23) yielded nearly pure albite (An < 1%). The plagioclase of the Eichigt aplite is nearly pure albite with ~1% anorthite.

As a peculiarity, a euhedral, turbid, and intensely altered (sericitized, albitized) plagioclase phenocryst, 3.2 x >8.5 mm in size (Pl-A_1?), was detected in thin section 15B. It contains a fine-grained "enclave" consisting of subhedral chloritized biotite + opaque minerals + quartz + euhedral apatite + radioactive accessory minerals, which resembles the Bt-A + quartz clusters. This grain is surrounded by a granophyric K-feldspar+quartz mantle (see Fig. 13a).

4.2.4 K-feldspar

Phenocrysts of the Kfs-A_1 generation are scarse. The single studied rounded grain (>12 mm in diameter, sample 11; see Figs. 2d, 14a) is considerably different in chemical composition compared to the widespread rectangular K-feldspar phenocryst population (Kfs-A_2). Optically homogeneous domains of the Kfs-A_1 core exhibit an albite content that averages to 11 %, possibly reduced by the strong perthitic albite exsolution lamellae, and contain some Ba (0.29 wt% BaO on average). The perthite-poor Kfs-rim is richer in the albite component (~ 26 % on average) and higher in Ba (0.52 wt% BaO on average; Fig. 10). In contrast, the K-feldspar of the fine-grained overgrowth of Kfs-A_1 is chemically similar to the more common Kfs-A_2 phenocrysts.

Kfs-A_2 grains poor in perthitic albite contain up to 14 w% albite (Ab). The maximum percentage of albite component measured was 33, possibly representing the original composition of the alkali feldspar solid solution. A single perthite-rich Kfs-A_2 phenocryst (sample 15) was observed that showed zoning with 8.4 % albite in the core and 4.1 wt% albite at the rim (Fig. 10). The low Ab content of the core may be due to the loss of Na by exsolution. The Ba (0.06 wt% BaO) and Sr (0.06 wt% SrO) contents in the core are little higher than at the rim (0.02 wt% and 0.03 wt%, respectively). On the other hand, the rim is richer in Rb (0.11 wt% Rb_2O) and P (0.14 wt% P_2O_5) relative to the core (0.02 wt% and 0.04 wt%, respectively).

The albite content of optical clear domains in the matrix kalifeldspar Kfs-B averages to 2.6 %.

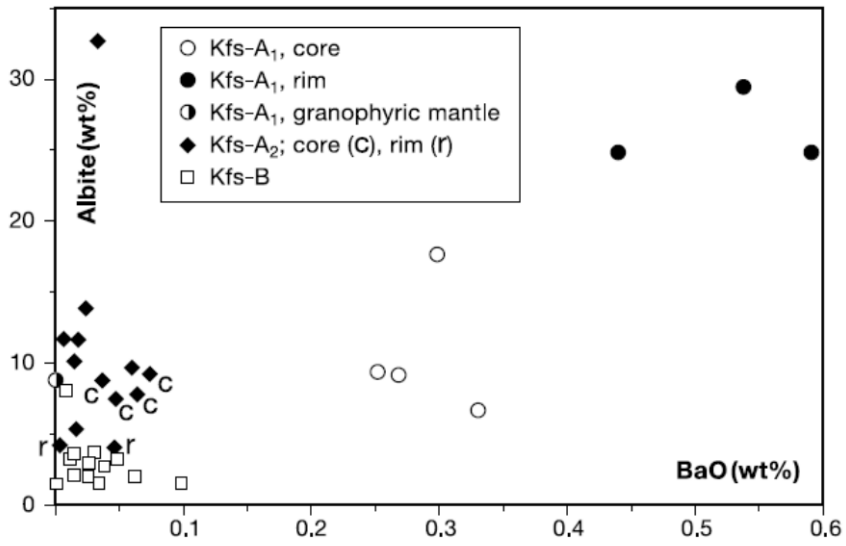

Fig. 10: Plot of albite component vs. BaO content of core, rim, and mantle of an early Kfs phenocryst (antecryst, Kfs-A_1), of core and rim of a late Kfs phenocryst (Kfs-A_2), and of the matrix Kfs (Kfs-B) from the Eichigt granite.

4.2.5 Quartz

SEM-CL imaging revealed a number of structures developed during crystal growth, secondary overprint and alteration. The observed features are illustrated schematically in Figure 11. Chronologic relationships of major events of quartz crystallization and alteration in the Eichigt granite are summarized in Table 8.

The rare and oldest quartz generation quartz A_1 (Qz-A_1) forms medium-sized (4-8 mm), partly rounded and embayed, and occasionally sharp-edged subhedral phenocrysts embedded in a fine- to medium- (to coarse-)grained groundmass. SEM-CL imaging reveals a very conspicuous complex concentric growth zoning of Qz-A_1 with strong CL contrasts (Figs. 11, 12a). Such CL-contrasted growth zoning is a feature common in phenocrysts in silica-rich igneous rocks (D'Lemos et al. 1997, Müller et al. 2002b, 2005, Wiebe et al. 2007). For Qz-A_1, a relatively low-luminescent, rounded core overgrown by bright-luminescent quartz with fine-scale oscillatory zoning is characteristic. The rounded core is commonly interpreted as a result of early magmatic quartz resorption because of the truncated older oscillatory growth zones (Müller et al. 2010). Lobate, worm-like embayments disturbing the planar growth of the crystal faces are developed in the bright oscillatory overgrowth (Fig. 11). The embayments are filled with fine-grained groundmass grains or overgrown by dull-luminescent and zoning-free groundmass quartz. Lobate growth embayments developed when foreign crystals, gas bubbles or immiscible melt droplets sticked on the growing crystal face and hindered the growth at this place (Laemmlein 1930, Kozlowski 1981, Lowenstern 1995, Müller et al. 2005). Subsequent growth zones adapt to the shape of the embayments, clearly indicating that these structures are not the result of quartz dissolution. However, in some cases, deuteric fluids entered the inner part

of phenocrysts via the embayments and overprinted partially the primary zoning along the embayments as illustrated in Fig. 11.

Table 7: Sequence of quartz crystallization in the Eichigt granite derived from microscopic and SEM-CL observations.

Stage	**Characteristics**
Quartz A_1 – early magmatic antecrysts	Nucleation and growth of subhedral phenocrysts exhibiting oscillatory and step zoning, resorption surfaces and lobate growth embayments, high CL contrast between step zones. Rare partly rounded and embayed, and partly sharp-edged sub-euhedral antecrysts, 48 mm in size, very complex concentric growth zoning with strong CL contrasts, relative low luminescent. Rounded crystal cores overgrown by bright luminescent quartz with fine-scale oscillatory zoning
Quartz A_2 – early magmatic phenocrysts	Sub-euhedral phenocrysts, 2–4 mm in size, with weakly CL-contrasted simple concentric growth. Zoning characterized by a rounded weak luminescent core and a slightly brighter overgrowth with lobate embayments. Forms clusters of 2–5 crystals.
Quartz B – matrix quartz	(Sub- to) anhedral quartz with low CL intensity without growth zoning and overgrowing phenocrysts. Some large crystals have slightly brighter luminescent crystal core.
Quartz C – phenoblastic matrix quartz	Anhedral, forms small rounded inclusions in other minerals or phenoblasts replacing feldspar and mica. Nearly no CL.
Quartz D_1 – intra-crystalline healed micro-fractures	Intense micro fracturing and precipitation of secondary quartz with very low CL intensity. Fracture width 2−10 μm.
Quartz D_2 – healed brecciated micro-veins	Micro-brecciation and precipitation of secondary quartz with very low CL intensity. Fracture width 20−100 μm

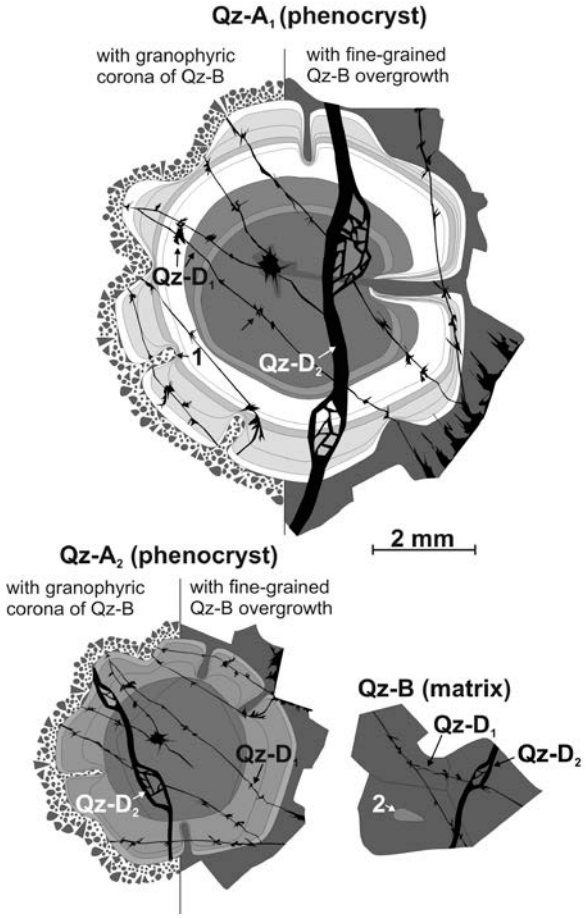

Fig. 11 Scheme of quartz generations and their growth and alteration structures revealed by SEM-CL in quartz of the Eichigt granite. Qz-A_1 − early quartz phenocrysts (antecrysts); Qz-A_2 − late quartz phenocrysts; Qz-B − matrix (groundmass) quartz; Qz-D_1 − secondary non-luminescent quartz forming healed micro cracks hosting secondary fluid inclusions; Qz-D_2 − secondary, non-luminescent quartz healing vein-like micro breccias. 1 − lobate growth embayment, 2 − small, bright luminescent cores in large Qz-B crystals, which may be interpreted as early nuclei.

Small sub-euhedral phenocrysts of quartz A_2 (Qz-A_2; 2 − 4 mm) with weakly CL-contrasted concentric growth zoning (Figs. 11, 12b) are much more common than Qz-A_1. The Qz-A_2 phenocrysts exhibit simple concentric growth zoning mainly characterized by a rounded weakly luminescent core and a slightly brighter overgrowth with weakly contrasted oscillatory zoning and lobate embayments (Fig. 12b). This type of zoning is typical for quartz phenocrysts of the Western Erzgebirge (Müller et al.2002a, 2003, 2010). Qz-A_2 commonly forms clusters of 2 − 5 crystals.

The matrix quartz B (Qz-B) forms sharp-edged fillings of interstices between older feldspars and micas, granophyric intergrowths with K-feldspar, and small-grained coronas around quartz and feldspar phenocrysts. The coronas are granophyric in the finer grained and granophyric granite varieties (Fig. 13a). Some of the larger Qz-B crystals contain small, slightly brighter luminescent cores, which may be interpreted as early nuclei formed prior to magma emplacement (number 2 in Fig. 11).

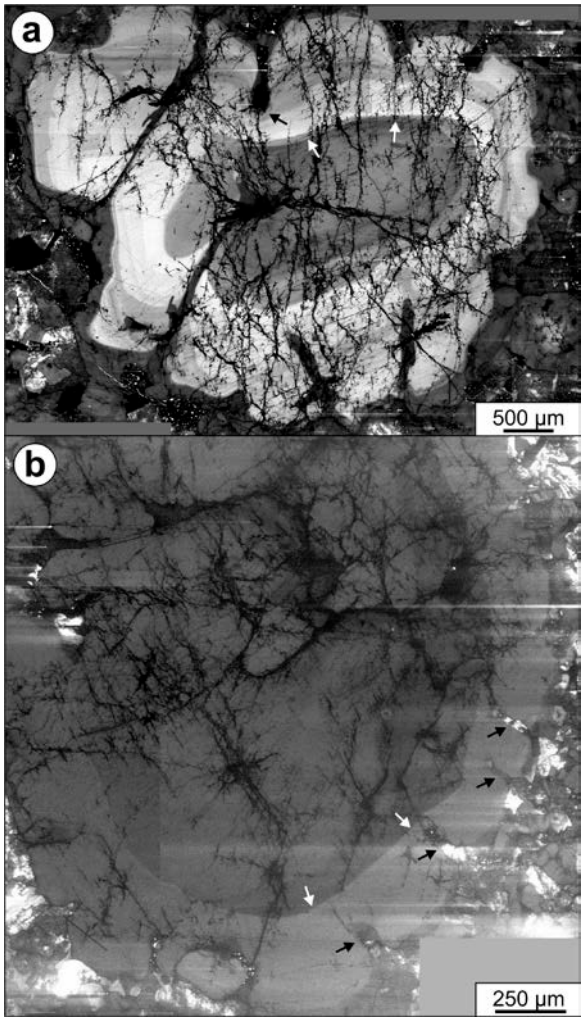

Fig. 12: SEM-CL images of zoned quartz phenocrysts. Lobate, worm-like growth embayments are characteristic. Arrows point to truncations. (a) Quartz A_1 phenocryst exhibiting strong CL contrasts with relatively low-luminescent rounded core and bright-luminescent finely zoned rim, interpreted as an antecryst (see section 5.2.1.5). (b) Weakly CL-contrasted quartz A_2 phenocryst with simple concentric growth zoning.

Quartz C (Qz-C) is a late generation corroding the earlier crystallized minerals. It is anhedral and forms small rounded inclusions in the outer parts of plagioclase phenocrysts. Qz-C replaces plagioclase (Fig. 13b) and K-feldspar grains, beginning at their grain boundaries (samples 16; 22) and proceeding to the formation of xenoblasts up to 2 mm in size, which may contain small skeletal relicts of feldspars and altered biotite (samples 12; 15). The late phenoblastic overgrowth and growth of Qz-C partially replacing other minerals indicates the presence of silica-oversaturated and water-enriched residual intrinsic melt in the final stage of granite solidification.

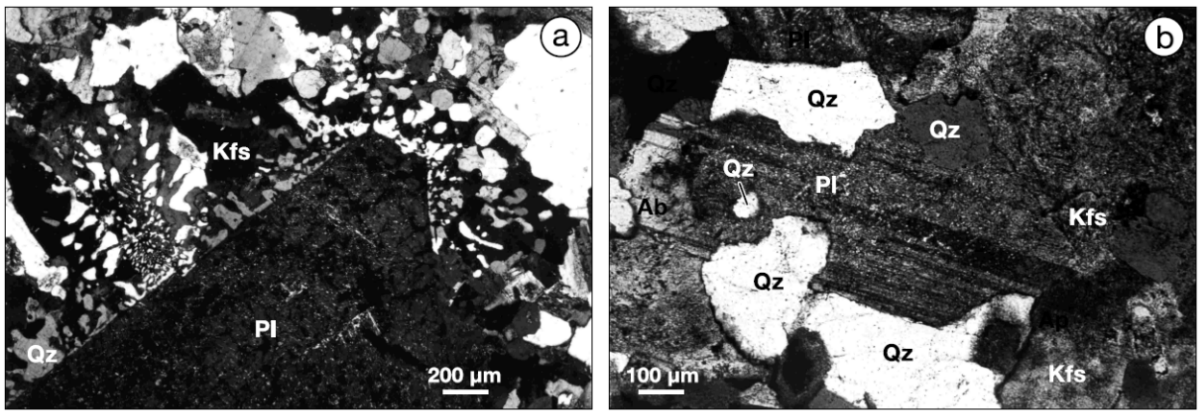

Fig. 13: (a) Part of a euhedral Pl phenocryst surrounded by a granophyric mantle of Qz and Kfs. − Crossed polars; thin section 15B. (b) Originally euhedral Pl locally with Ab rim and corroded by Qz-C. − Crossed polars; thin section 22.

Qz-A_1 to Qz-C are followed by two types of intra-crystalline secondary structures (quartz D_1 and quartz D_2: Qz-D_1, Qz-D_2) which can be visualized by CL only (Figs. 11, 12). These structures developed after granite solidification. Qz-D_1 commonly forms thin irregularly healed micro-cracks (2 − 10 µm wide) connecting small, normally star-like quartz domains. These structures are almost non-luminescent and, thus, appear black in the SEM-CL images, and host secondary fluid inclusions. Such dense networks of healed cracks connecting low-luminescent quartz domains are a widespread phenomenon in quartz of granitic rocks (Sprunt & Nur 1979, Behr & Frentzel-Beyme 1989, Valley & Graham 1996, D'Lemos et al. 1997, Müller et al. 2000, Van den Kerkhof & Hein 2001). This micro-fracturing can be related to internal stresses at grain scale, resulting from the strong thermal contraction of quartz relative to the feldspar framework in the slowly cooling granite magma (VOLLBRECHT et al. 1991, 1994).

Some quartz crystals exhibit broad-healed cracks (20 − 100 µm; quartz D_2; Qz-D_2) containing small fragments of older quartz (Fig. 11). This micro-brecciation is related to a relative young stress-inducing event, possibly the regional polymetallic-fluorite mineralization.

4.2.6 Topaz

Topaz rarely occurs as small euhedral or subhedral crystals (about 0.1 − 0.2 mm) mostly included in feldspars (Fig. 14b). More frequently it precipitated as anhedral grains (0.2 − 0.5 mm) in interstices between magmatic minerals, as anhedral-blastic grains (up to 0.8 mm; Fig. 14c) often associated with biotite-C, or in vug-like aggregates together with quartz (Fig. 14d). These overall textural patterns suggest a late-magmatic origin of this topaz (cf. Gioncada et al. 2014, Agangi et al. 2014).

Chemically, the topaz of the Eichigt granite is a normal F-topaz, with F contents of ~ 18.5 wt%. One grain was measured that exhibited a weak compositional zoning, with a little lower F content in the core (Table 8), a feature also noticed by Agangi et al. (2014).

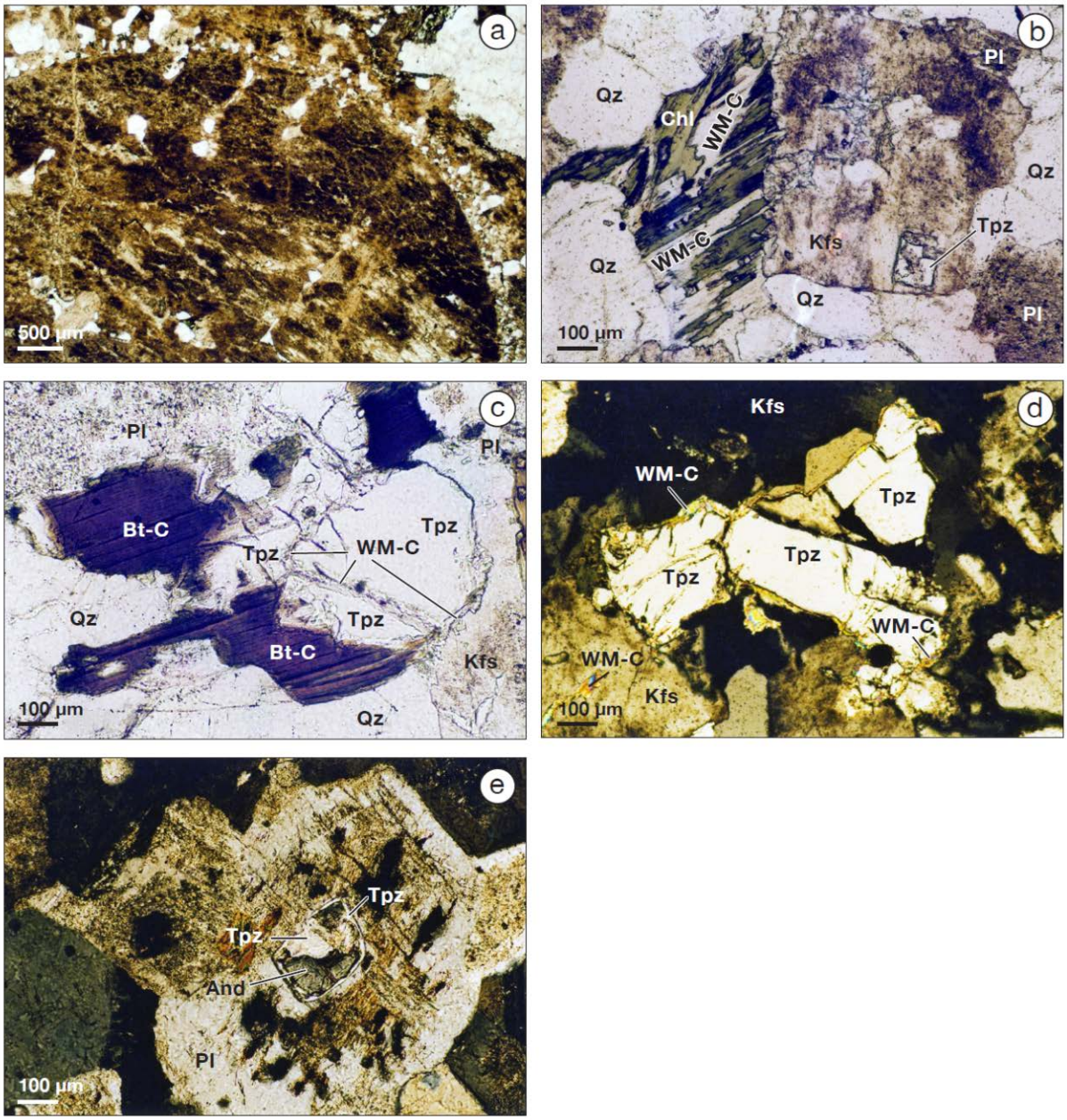

Fig. 14: Photomicrographs of the Eichigt granite: (a) A part of a rounded Kfs-A_1 phenocryst (antecryst; altered, brown). It contains inclusions of Qz and mica. The core is rich in vein perthite, the rim (dark) is poorer in perthite. The rounded grain rim is sharply accentuated by a fine-grained Kfs–Qz mantle. − Plane-polarized light; thin section 11A. (b) Euhedral Tpz included in Kfs. Left of this Kfs is an altered biotite grain consisting of chlorite and WM-C. − Plane-polarized light; thin section 23. (c) Large anhedral Tpz grain intergrown with fresh Bt-C. Secondary WM-C crystallized on the surface and in fissures of the Tpz. − Plane-polarized light; thin section 15A. (d) Vug-like Tpz–Qz aggregate, Tpz with narrow domains of WM-C precipitating on the surface and in fissures. − Plane-polarized light; thin section 23. (e) Plagioclase-hosted andalusite corroded by Tpz and overgrown by a small Tpz mantle. − Crossed polars; thin section 15B.

4.2.7 Andalusite

Andalusite occurs as small grains (100 − 250µm) of variable shape: (a) as originally euhedral-prismatic single grains in plagioclase now marginally altered to white mica (sample 15B/6), (b) as anhedral relictic grains included in muscovite (sample 19), and (c) as anhedral grains with microcracks

surrounded by a fine rim (5−10µm) of white mica and irregularly shaped opaque minerals hosted in plagioclase (15B/3).

Whereas the alteration of andalusite to white mica is widespread in granitic rocks, its topazation as observed in sample 15 is uncommon (Fig. 14e). This fact implies that andalusite was instable in the Eichigt granite magma.

Results of EMP-analyses of andalusite are compiled in Table 8. Except the major components Al and Si, Fe constitutes the only element present at concentrations > 0.1 wt%. Owing to the paucity in Fe, the Eichigt andalusite is colorless and can be easily misidentified optically for topaz.

Table 8: Results (wt%) of electron-microprobe analyses of topaz and andalusite

	Topaz					Andalusite		
Sample No.	15	23	23	Average	1σ	15	Average	1σ
Spot No.	Tpz 1/9	Tpz 4/7	Tpz 4/10	n = 75		And 6/1	n = 18	
		Core	Rim					
SiO_2	33.0	32.9	33.1	33.0	0.16	36.9	36.9	0.26
TiO_2	0.03	b.d.	0.01	0.01	0.01	b.d.	0.02	0.02
Al_2O_3	55.3	54.9	55.3	55.3	0.21	62.7	62.4	0.55
FeO[a]	0.02	0.03	0.02	0.02	0.02	0.41	0.43	0.09
MnO	0.02	0.04	b.d.	0.01	0.01	b.d.	0.01	0.02
MgO	b.d.	0.02	0.01	b.d.	0.01	b.d.	b.d.	
CaO	0.02	0.01	0.02	0.01	0.01	0.01	0.01	0.01
F	18.6	18.1	18.6	18.5	0.23	b.d.	b.d.	
Cl	b.d.	b.d.	b.d.	b.d.		b.d.	b.d.	
H_2O[b]	1.03	1.17	1.02	1.06	0.12			
Sum	107.9	107.1	108.0	107.9		100.0	99.8	
O=(F+Cl)	7.81	7.63	7.82	7.79				
Total	100.1	99.5	100.2	100.1				

[a] = total Fe as FeO; [b] = determined stoichiometrically; b.d.= below detection limit

4.2.8 Chlorite

The chemical composition of chlorite is reported in Table 9. Fluorine, Cl, and Ba contents are notoriously < 0.1 wt%. All analyzed chlorite grains are trioctahedral and Fe-dominant as typical for chlorite from felsic rocks (Zane et al. 1998). They classify as chamosite following the nomenclature for trioctahedral chlorites proposed by Bayliss (1975) and accepted by the "Association Internationale pour l' Etude des Argiles" (AIPEA) Nomenclature Commission (Bailey 1980, 1988).

Compared to data in the literature the X_{Fe} values of the Eichigt granite chlorites are high. After Zane et al. (1998) intermediate X_{Fe} values – about 0.45 − 0.61 in their Fig. 6d – are characteristic for chlorites from felsic rocks. The chlorites from the non-albitized common Eichigt granite have X_{Fe} = 0.82 − 0.87. This is very high. X_{Fe} values ≥ 0.8 are uncommon and seldom noted in the literature, e.g. Zang & Fyfe (1995), Zimák (1999), Zhao et al. (2005). Apparently, these X_{Fe} values reflect the likewise high X_{Fe} ratio from the precursor mineral of the chlorite, namely biotite with X_{Fe} = 0.903 on

average (Table 5). The ratio X_{Fe} = Fe/(Fe + Mg) of normal-granite chlorite (sample 11B) is significantly higher (Table 9) than that of chlorite from the albitized granite (0.61 – 0.75; sample 12). The latter chlorite is also compositionally more variable. This mainly applies to the contents of Fe, Mg, and, less significantly, Mn (Table 9). The lower Fe content is presumably caused by selective Fe removal during albitization.

Table 9: Results (wt%) of EMP-analyses of chlorite

Sample No.	11B				12			
Spot No.	Chl 1/6	Chl 2/1	Average n = 9	1σ	Chl 4/2	Chl 2/3	Average n = 15	1σ
SiO_2	23.9	23.8	24.0	0.31	25.1	24.0	25.2	0.63
TiO_2	0.06	0.03	0.10	0.05	0.03	0	0.03	0.01
Al_2O_3	19.5	19.2	19.8	0.35	20.1	20.4	20.0	0.30
FeO	41.3	41.0	40.9	0.60	34.7	36.6	34.1	1.70
MnO	1.31	1.43	1.38	0.09	1.70	2.25	1.92	0.22
MgO	3.89	4.71	4.25	0.38	8.58	6.78	9.13	1.44
CaO	0.02	0.01	0.02	0.01	0.03	0.01	0.02	0.02
Na_2O	0.06	0	0.03	0.02	0.03	0.02	0.02	0.01
K_2O	0.06	0.03	0.10	0.12	0.02	0.02	0.02	0.01
total	90.1	90.2	90.6		90.3	90.1	90.5	
Fe/(Fe+Mg)	0.86	0.83	0.84	0.01	0.69	0.75	0.68	0.05

4.2.9. Other accessory minerals

Granite and aplite from Eichigt contain the identical assemblage of radioactive accessory minerals, namely zircon, monazite-(Ce), xenotime-(Y), thorite, uraninite, and synchysite-(Ce). But they differ in the absolute abundance of the individual species. In contrast to the granite, the aplite is relatively rich in thorite, hosts modest amounts of zircon and uraninite, but is poor in monazite-(Ce) and xenotime-(Y), which are tiny grains to small to permit analysis with the electron microprobe. The presence of synchysite-(Ce) is a distinguishing signature of granite and aplite from this study. It forms either small anhedral solitary crystals or, more typically, large anhedral masses of several 100µm in size. Moreover, as a rarity, a single grain of strongly altered fergusonite-(Y), ideally $YNbO_4$, was identified in the albitized granite sample 12. To demonstrate the general compositional patterns of these all these species, a selection of microprobe data is compiled in Table 10. A comprehensive survey of the composition and conditions of formation of the radioactive accessory minerals from Eichigt is, however, beyond the scope of this contribution.

Additionally to these accessories, the Eichigt granite contains a relatively small amount of apatite. It occurs in tiny needles (~5 x 70 µm) included in feldspars and quartz and eu- to subhedral columns

(~20 − 90 x 80 − 200 µm) preferentially hosted in biotite A-rich clusters. In the aplite, sparse granules of eu-to subhedral hexagonal or rounded apatite occur, mostly only 10 − 30µm in size (Fig. 4c).

Table 10: Representative results of EPM analyses (wt%) of accessory mınerals

	granite					aplite		
Sample No.	11	11	11	12	11	29	29	29
Mineral	zircon	monazite-(Ce)	xenotime-(Y)	fergusonite-(Y)	synchysite-(Ce)	zircon	thorite	synchysite-(Ce)
P_2O_5	0	29.52	34.13		0	0	4.06	0
Nb_2O_3				42.39				
Ta_2O_3				1.68				
SiO_2	32.33	0.55	0.37	2.11	0.10	29.26	15.15	0.13
TiO_2				1.13			0.04	
ZrO_2	66.05					55.54	0	
HfO_2	1.80					6.12	0	
ThO_2	0	7.70	0.53	2.05	0	0.35	51.83	0
UO_2	0	0.99	0.80	0.72	0	0.86	10.75	0
Al_2O_3	0				0	0.11	0.27	0
Sc_2O_3	0					0.04		
Y_2O_3	0	2.12	41.10	22.29	3.40	0.19	4.83	1.03
La_2O_3		9.91	0.04	0.06	12.43		0.05	12.83
Ce_2O_3	0	25.96	0.22	0.47	23.39	0	0.33	24.57
Pr_2O_3	0	3.13	0.06	0.10	2.34		0.16	2.56
Nd_2O_3	0	11.96	0.52	0.35	8.16	0	0.48	9.89
Sm_2O_3	0	3.03	0.56	0.40	1.46	0	0.30	1.67
Gd_2O_3	0	2.06	3.37	2.07	1.46	0	0.78	1.12
Tb_2O_3		0.19	0.77	0.55	0.17		0.04	0
Dy_2O_3	0	0.65	5.37	3.33	0.68	0.10	0.74	0.10
Ho_2O_3		0.06	1.16	0.81	0.09		0.11	0
Er_2O_3	0	0.19	4.34	2.60	0.16		0.34	0
Tm_2O_3			0.64					
Yb_2O_3	0.05	0	4.20	2.39	0.11	0.36	0.35	0
Lu_2O_3		0	0.53	0.35	0			0
CaO	0	1.77	0.04	2.10	17.39	0.24	1.79	17.53
FeO	0		0	0.83	0.23	3.28	0.51	
PbO	0	0.15	0		0	0	0.02	
MnO				0.53				
Na_2O				0.14				
F	0	0	0		3.04	0	0.41	4.04
$F=O_2$					1.28		0.17	1.70
total	100.22	99.93	98.75	89.43	73.34	96.82	93.14	73.76

4.3. Whole-rock geochemistry

Virtually unaltered samples characterize the Eichigt granite (K > Na) as an evolved, mildly peraluminous (A/CNK = 1.18 – 1.21), high-Si (SiO_2 = 75 – 76 wt%) biotite monzogranite (Table 12). The granite is poor in P and contains moderate concentrations of F (0.20 – 0.28 wt%). Chondrite(CN)-normalized REE patterns are weakly declined (La_{CN}/Lu_{CN} = 3.9 – 4.3) and display moderately deep negative Eu-anomalies (Eu/Eu* = 0.11 – 0.18). Despite its silica-rich nature, the granite is poor in several lithophile elements, particularly in those preferentially bound in micas (Li, Cs). It is remarkably poor in Sn (5 – 7 ppm), but possesses a moderate enrichment in W (10–12 ppm) (W/Sn >

1). The concentrations of the actinide elements Th and U also are at a moderate level. Noteworthy are elevated concentrations of Y (59 – 75 ppm) and Pb (47 – 56 ppm). The granite shows fractionated Zr/Hf ratios (23 – 25), whereas the ratio of Y/Ho is chondrite-like (27 – 28). Altogether, the Eichigt granite classifies within the group of medium-F, low-P biotite granites according to the subdivision scheme elaborated by Förster et al. (1998, 1999) for the Erzgebirge–Vogtland Zone granites.

Table 11: Bulk-rock geochemistry of the Eichigt granite and aplite from borehole 2072/72

Rock	Granite				aplite	
Sample No.	21	22	19	15	30	29
SiO_2 (wt%)	74.6	76.1	76.2	75.0	74.8	74.6
TiO_2	0.14	0.11	0.10	0.10	0.01	0.01
Al_2O_3	13.4	12.9	12.9	13.5	15.4	15.1
$Fe_2O_3^*$	1.83	1.58	1.49	1.69	1.02	1.07
MnO	0.03	0.03	0.03	0.03	0.01	0.01
MgO	0.11	0.11	0.10	0.09	0.13	0.12
CaO	0.45	0.45	0.51	0.57	0.28	0.32
Na_2O	2.63	2.80	2.60	2.95	3.90	4.71
K_2O	5.55	5.06	5.02	5.02	2.74	2.19
P_2O_5	0.10	0.11	0.11	0.11	0.11	0.12
H_2O^+	0.89	0.79	0.81	0.90	1.55	1.72
CO_2	0.29	0.17	0.21	0.26	0.28	0.27
F	0.20	0.23	0.28	0.23	0.12	0.11
$O=F_2$	0.08	0.10	0.12	0.10	0.05	0.05
Total	100.1	100.3	100.2	100.3	100.3	100.3
Li (ppm)	17	17	42	50	10	7.2
Be	3.7	4.2	4.5	5.2	4.2	4.5
Sc	7.9	7.2	6.9	8.3	1.4	0.85
V	<10	<10	<10	<10	<10	10
Cr	<10	<10	<10	<10	<10	<10
Ni	<10	<10	<10	<10	<10	<10
Zn	30	34	38	36	18	19
Ga	22	20	21	22	23	22
Rb	389	369	401	412	260	206
Sr	49	33	32	31	34	36
Y	75	62	59	70	5.9	4.4
Zr	103	86	87	86	12	16
Nb	24	21	21	21	21	31
Mo	1.4	1.5	1.3	2.5	0.73	1.8
Cd	0.28	0.27	0.27	0.32	0.12	0.16
Sn	7.1	6.4	5.4	6.5	17	15
Sb	0.14	0.10	0.08	0.12	0.46	0.14
Cs	9.3	10.0	15.3	17.7	5.1	7.0
Ba	487	144	115	112	70	86
La	47.5	37.1	35.5	32.7	5.1	5.1
Ce	108	85.7	82.6	75.6	10.1	9.2
Pr	13.2	10.6	10.2	9.4	1.1	0.93
Nd	49.6	39.6	38.1	34.8	3.6	2.9
Sm	11.8	9.8	9.5	9.0	1.2	0.93
Eu	0.69	0.36	0.35	0.35	0.031	0.046
Gd	11.4	9.1	9.1	9.2	0.95	0.81
Tb	2.0	1.7	1.6	1.8	0.18	0.15
Dy	13.2	11.2	10.6	11.9	1.1	0.95
Ho	2.7	2.3	2.2	2.5	0.19	0.18
Er	8.3	7.0	6.5	7.7	0.59	0.54
Tm	1.2	1.0	0.98	1.1	0.11	0.10

Yb	8.0	6.9	6.5	7.8	0.91	0.75
Lu	1.1	0.98	0.90	1.1	0.13	0.11
Hf	4.1	3.8	3.8	3.6	0.37	0.35
Ta	3.4	2.2	3.0	2.9	5.1	12
W	12	12	12	10	12	11
Tl	1.6	1.5	1.6	1.6	0.68	0.55
Pb	51	47	51	56	6.0	215
Bi	0.04	0.18	0.05	0.04	0.92	1.9
Th	23.7	19.8	19.3	18.2	18.3	7.6
U	10.6	7.6	10.6	8.5	22.8	10.6
A/CNK	1.20	1.18	1.21	1.19	1.56	1.41
K/Rb	118	114	104	101	87	88
Rb/Sr	8.0	11.1	12.5	13.5	7.7	5.7
Y/Ho	27.5	27.0	27.4	28.3	30.8	25.1
Zr/Hf	24.9	22.9	23.0	24.0	32.6	44.0
Th/U	2.2	2.6	1.8	2.1	0.8	0.7
Nb/Ta	7.0	9.3	6.9	7.1	4.1	2.6
La_{CN}/Lu_{CN}	4.3	3.9	4.0	3.9	4.0	3.1
Eu/Eu*	0.18	0.11	0.11	0.12	0.09	0.16

[a] = total Fe as Fe_2O_3, A/CNK = molar $Al_2O_3/(K_2O+Na_2O+CaO)$, CN = chondrite, $Eu/Eu^* = Eu_{CN}/(0.5Sm_{CN} + 0.5Gd_{CN})$.

The aplites classify as highly evolved (Na > K), strongly peraluminous, feldspar-rich and biotite-devoid monzogranites (cf. Table 5). Compared to the granite, they are distinctly poorer in a number of elements, in particular in such hosted in accessory minerals (Ti, Zr, Hf, Y, REE) and micas (Li, Rb, Cs, F). In contrast, they are richer in Sn (15 – 17 ppm) relative to the granite, at virtually the same concentrations of W (W/Sn < 1). Granite and aplites exhibit similarly shaped REE patterns. Contrasting concentrations of Nb, Pb, Th, and U between the two aplites suggest either the influence of alteration and/or contamination processes or, more likely, that both were expelled from the granite magma at slightly different times of its evolution.

4.4. Age

The presence of virtually unaltered uraninite in both the granite and aplites provided the opportunity to determine “chemical” ages of low standard deviation from electron-microprobe data (Charoy 1986, Bowles 1990). Uraninite has been multiply demonstrated to yield precise and robust ages for peraluminous granites from the Erzgebirge-Vogtland (Förster 1999; Kempe 2003; Romer et al. 2007; Förster et al. 2008). Single-point Th−U−total Pb uraninite ages were calculated using the constants of Steiger & Jäger (1977) for the radioactive decay of Th and U.

The data reported in Table 12 indicate that the granite and aplite are coeval. A total of six single-spot analyses of uraninite and granite and aplite resulted in a combined weighted mean Th–U–total Pb age of 305.3 ± 4.1 Ma (2σ; MSWD = 0.104), assuming a constant error of ± 10 Ma, applying the ISOPLOT/EX program of Ludwig (1999). Applying the same procedure to uraninite from both aplite and granite from Schönbrunn would yield a mean age of 305.7 ± 3.2 Ma (2σ, n = 10), indicating the both apical intrusions emplaced simultaneously. Combining the uraninite data from Eichigt and

Schönbrunn imply an emplacement age of the concealed massif of 305.6 ± 2.5 Ma (2σ, MSWD = 0.116, n = 10) (Fig. 15),

Table 12: Composition (wt%) and apparent Th−U−total Pb single-point ages of uraninite from Eichigt

	granite	aplite				
Sample No.	16	29	29	29	30	30
ThO_2	12.53	12.87	10.79	11.73	7.99	12.53
PbO	3.67	3.62	3.72	3.61	3.71	3.67
UO_2	83.23	81.99	84.83	82.72	86.44	82.97
Age (Ma)	305.9	305.7	306.4	303.8	302.9	307.1

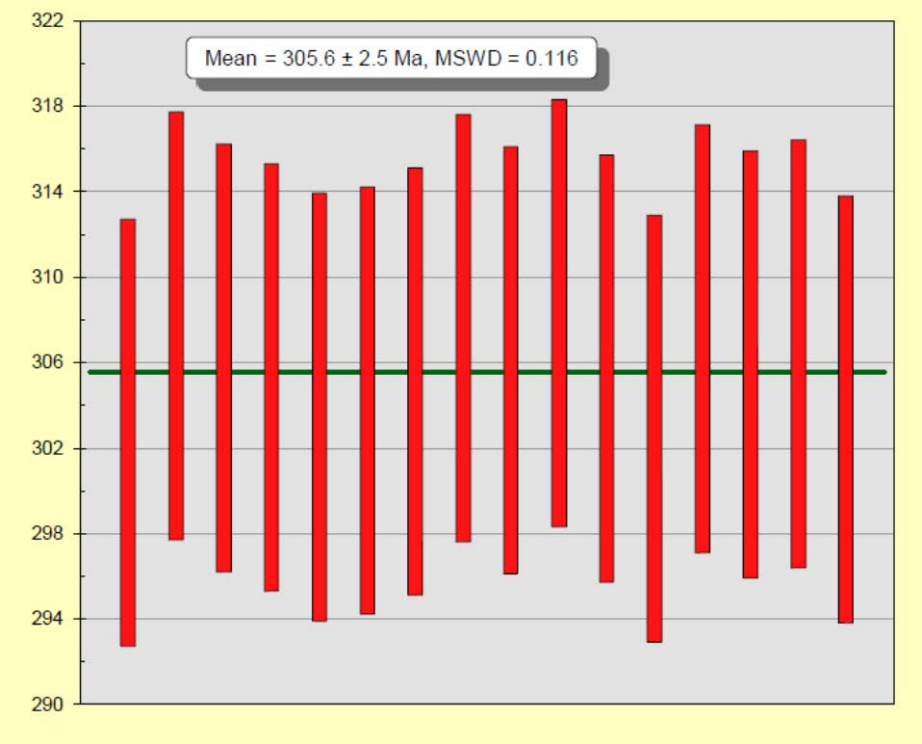

Fig. 15: Calculated Th−U−total Pb single-point ages (with 10 Ma error bars) and weigthed mean age (2σ) of uraninite from granites and aplites of the Eichigt−Schönbrunn granite massif, using the Isoplot/Ex program of Ludwig (1999). MSWD = mean standard weighted deviation.

5. Discussion

5.1 Chemical classification of the Eichigt granite

Geochemically, the Eichigt granite resembles evolved granites of the post-collisional aluminous A-type class. According to the granite nomenclature elaborated for the Erzgebirge–Vogtland metallogenic province (Förster et al. 1996, 1999), the granites from Eichigt as well as Schönbrunn classify as medium-F, P-poor biotite granites. The spatially closest representative of this group is the

rhyolite/microgranite association at Gottesberg (Gottesmann et al. 1995, Förster et al. 2007), some 25 km NE of Eichigt (see Fig. 1).

5.2 The Eichigt granite in relation to other granites of the Erzgebirge–Vogtland province

Minerals forming solid solution systems, such as micas and topaz, are suitable for studying the relations of the Eichigt granite with the neighbouring granite massifs.

Comparing the chemical composition of the trioctahedral micas from the Eichigt granite with those of trioctahedral micas from the adjacent F-poor biotite granites, medium-F biotite granites/rhyolites, F-poor two-mica granites, and F–P-rich Li-mica granites of the Erzgebirge–Vogtland (Fig. 16), it is obvious that the Eichigt micas display the strongest affiliation with trioctahedral micas from the Gottesberg microgranites (Förster et al. 1995, Gottesmann et al. 1996) and the least-evolved subintrusions of the multi-phase F–P-rich Li-mica granite massifs, such as Eibenstock. This correspondence is in agreement with the whole-rock chemical composition of the Eichigt granite in relation to the Gottesberg rhyolite/microgranite association (*cf.* section 5.1). However, both magmatic suites are chemically similar, but not identical. Thus, the Gottesberg association is distinctly richer in certain accessory mineral-bound elements, such as Zr, Hf, Nb, Ta, Th, and U (Förster et al. 2007).

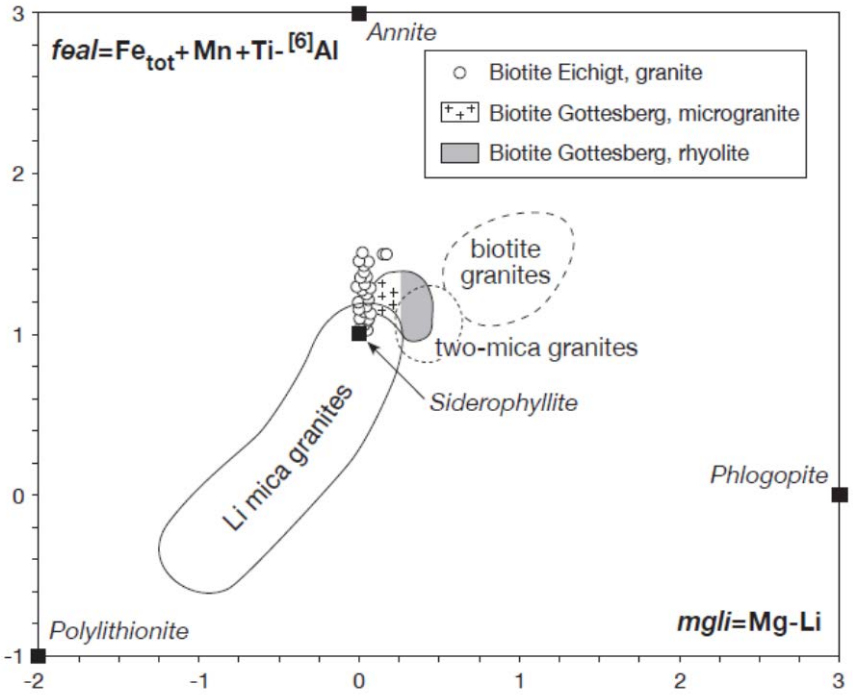

Fig. 16: Position of biotite (siderophyllite) from the Eichigt granite in comparison to trioctahedral micas of other granitic rocks from the Westerzgebirge−Vogtland, plotted in the *feal/mgli* (in *apfu*) mica diagram elaborated by TISCHENDORF et al. (1999b; 2004).

The F content of the late-magmatic topaz from the Eichigt granite – on average 18.5 wt% − is lower than that of most other topaz-bearing granitic rocks from the Erzgebirge−Vogtland. These include representatives of the F−P-rich Li-mica granite group, such as the granites from Ehrenfriedersdorf (18.3 − 19.1 wt% F; Thomas 1982), Eibenstock (19 − 21 wt% F; Förster et al. 1999), and Podlesí (18.9 − 19.6 wt% F; Breiter 2002, Breiter & Kronz 2004), as well as granites assigned to the F-rich, P-poor Li-mica granite group, such as Altenberg (coarse-grained quartz−topaz−zinnwaldite rock: ~19.3 wt%, Breiter et al. 2013) and Cinovec (albite–zinnwaldite granite: 19.5 − 19.8 wt%, Breiter et al. 2013). Although F_{topaz} and $F_{whole\ rock}$ are not strongly correlated (*cf.* Breiter & Kronz 2004), the relatively lower F content of the Eichigt topaz suggest a relatively lower F concentration of the melt, from which the Eichigt granite crystallized. This would be in agreement with the striking differences in bulk-rock F contents between Eichigt and the above listed granites.

5.3 Genetic relations between granite and aplites

The granite and the aplites are spatially associated and coeval, suggesting that they are also cogenetic. However, several compositional features suggest that (a) both aplites are not derivatives of the same magma batch (cf. chapter 4.3) and (b) that they do not simply represent residual melts exsolved from the crystallizing Eichigt granite magma. The most serious parameter opposed to the residual-melt hypothesis is the Zr/Hf ratio, which is relatively resistant even against severe overprinting. It has been multiply demonstrated that progressively crystallizing magmas yield residual melts with lower Zr/Hf ratios, owing to the preferred substitution of Hf relative to Zr in subsequently precipitating generations of zircon (e.g., Zaraisky et al. 2009, and references therein). This pattern is just the opposite observed at Eichigt, where the aplites have substantially greater Zr/Hf ratios than the neighbouring granite.

5.4 Indications for magma mingling

There are several indications that magma mingling may have played a minor role in the formation of the Eichigt granite magma. Generally, the importance of mixing/mingling and the possibly associated hybridization is well accepted in igneous petrology (e.g., Vernon 1990, Barbarin 1991, Hibbard 1991, Cox et al. 1996, Baxter & Feely 2002, Słaby et al. 2007a, b). Grogan & Reavy (2002) referred to the fact that in addition to the widespread felsic-mafic magma mixing/mingling, felsic-felsic magma mixing/mingling does also occur. It is particularly significant in the understanding of the crystallization of peraluminous granitiods. Felsic-felsic magma mixing may develop as mixing process of granitic melts from different sources or batches of melts from the same magma chamber. It can produce disequilibrium structures caused by changes of the chemical composition or physical conditions of the magma, for instance by diffusion, by variation of the water content, or by undercooling of the system resulting in different rates of nucleation and crystal growth.

In case of the Eichigt granite, special mineral-structural features, peculiarities in the mineral chemistry, and the presence of minerals less common in granites point to felsic-felsic magma mingling involved in the evolution of the magma.

Special mineral-structural features suggesting magma mingling include CL-SEM observations on quartz phenocrysts from the Eichigt granite. The early magmatic Qz-A_1 phenocrysts (see section 4.2.5 and Figs. 11-12), which are rare compared to Qz-A_2 phenocrysts, may not be phenocrysts in the strict sense. They have rounded cores resulting from magmatic resorption, implying early magma mingling. Therefore, Qz-A_1 and Qz-A_2 may not have shared a common history. Namely, Qz-A_1 did not crystallize from the melt, in which it is now hosted. Rather it represents a crystal cargo coming from another felsic melt that mingled with the host granite magma (Davidson et al. 2007). Qz-A_1 phenocrysts are not xenocrysts accidentally incorporated from unrelated wall rocks, as they are grown and recycled from genetically closely related progenitor magmas. W.E. Hildreth (pers. Comm. in Davidson et al. 2007) suggested the term “antecryst” to denote a mineral that originated in the magma system, but does not represent a true phenocryst (cf. Charlier et al. 2005). Davidson et al. (2007) proposed that magmatic rocks can be represented by mixtures of melts, recycled antecrysts, and true phenocrysts. Regarding the Eichigt granite, we suppose that the rare Qz-A_1 grains are antecrysts and the dominant early magmatic Qz-A_2 grains represent true phenocrysts.

The strong CL-intensity contrast between different growth zones and the generally high CL intensity of the Qz-A_1 antecrysts from the Eichigt granite are atypical for quartz phenocrysts from granitic rocks of the Western Erzgebirge/Krušne Hory, whereas the Qz-A_2 phenocrysts show growth structures typical for these granites (Müller et al. 2002a, 2003, 2010). The CL intensity of igneous quartz is mainly related to the concentration of Ti (Müller et al. 2000, 2002b, Wark et al. 2007, Wiebe et al. 2007). The Ti concentration in quartz in turn is a function of its temperature and, to a minor extent, pressure of crystallization (Wark & Watson 2006, Huang & Audétat 2012). Thus, Qz-A_1 was presumably exposed to strongly varying crystallization temperatures during crystal growth.

The rare K-feldspar phenocrysts Kfs-A_1 with a pronounced rounded grain shape (see section 4.2.4 and Figs. 2d, 14a) and a relatively high Ba content (Fig.10) may have also grown differently. These Kfs phenocrysts could have originated from an earlier, Ba-richer magma batch that subsequently mingled with the felsic melt now representing the Eichigt granite. After being uptaken by the Eichigt magma, the Kfs-A_1 grains were partly resorbed, got their rounded shape, and finally a granophyr-like Qz + Kfs rim. A similar scenario has been described by Cox et al. (1996), Gagnevin et al. (2005) and Słaby et al. (2007a, b), who recognized the particular genetic importance of the Ba content of K-feldspars. Summarizing, the rounded Kfs-A_1 phenocrysts also appear to represent antecrysts.

The conspicuous clusters of accessory mineral-rich ragged biotite-A rich in quartz (Fig. 4e) may as well constitute antecrysts. These Bt-A clots, probably grown in an earlier granitic magma batch, are now in a stage of incomplete equilibration with the host magma. This is implied by (i) the diffuse

margins of the clusters, (ii) the intense corrosion of the biotite by quartz, without chloritization or muscovitization of the biotite.

The ideally euhedral plagioclase phenocryst (see Fig. 13a) with a small Bt + Qz + accessory mineral enclave (see chapter 4.2.3), resembling the Bt-A + Qz clusters, may also be an antecryst rather than a true phenocryst. It is mantled by granophyric Qz + Kfs, like antecrysts of Qz-A_1 and Kfs-A_1.

One mineral in the Eichigt granite, which is generally not widespread in granites, is andalusite. After Clarke et al. (2005), andalusite could represent a primary magmatic phase in granites. Indeed, the frequently euhedral-prismatic shape of andalusite in the Eichigt granite argues for crystallization from the melt. Clarke et al. (2009) showed experimentally that primary andalusite can form from a water-saturated peraluminous melt with fluorine ≤ 1 wt% at T ≥ 650°C. Remarkably, the andalusite is often included within weakly regularly zoned plagioclase. Andalusite (or plagioclase + included andalusite) may have been formed within an F-poorer forerunner magma portion that got mixed with the water- and F-richer magma (note the presence of topaz) that finally gave rise to the Eichigt granite. In this environment, andalusite became instable and was converted to topaz (Fig. 14e) and, at a later stage, to white mica. Presumably, a certain percentage of the observed pinitic pseudomorphs also originated from andalusite breakdown.

5.5 Chlorite geothermometry

Among others, the chemical composition of chlorite is a function of temperature. Accordingly, few octahedral vacancies, relatively large contents of (Fe + Mg), tetrahedral Al, and total Fe would imply that chloritization of the Eichigt granite occurred already early post-magmatically, i.e., at relatively high temperatures. Various equations were formulated to calculate the chlorite formation temperatures (cf. Cathelineau & Nieva 1985). These empirical chlorite geothermometers are calibrated on the basis of fluid-inclusion studies, direct temperature measurements in geothermal wells, or by comparisons with other mineral geothermometers (Kranidiotis & MacLean 1987, Cathelineau 1988, Jowett 1991, Hillier & Velde 1991, Zang & Fyfe 1995, FrimmeL 1997, Xie et al. 1997, Ruggieri et al. 2006).

Application of these geothermometers to the chlorites from Eichigt yield a temperature range of *ca.* 290° – 370°C, excluding the extremely low and geologically unreasonable values of ca. 130° – 190°C that would result from application of the Xie et al. (1997) equation. Noteworthy, calculated formation temperatures of the chemical different chlorites from the fresher Eichigt granite (X_{Fe} = 0.84) and from the albitized Eichigt granite (X_{Fe} = 0.68) are virtually corresponding. This fact and the relatively wide range of the calculated temperature values imply that T-information obtained from the empirical chlorite geothermometry should be used with caution. It has to be taken into account that additional factors exert control on the formation temperature of chlorite, e.g., Fe_{total} and Fe^{3+} content of the chlorite, bulk composition of the host rock (Zane et al. 1998), mineral assemblage, pressure,

oxygen fugacity, pH (De Caritat et al. 1993, Zane et al. 1998), chlorite precursor mineral, and contamination (Jiang et al. 1994).

Recently, Bourdelle et al. (2013) compared the suitability of various chlorite geothermometers. They confirmed the general link between composition and formation temperature. However, these authors figured out that most of the empirical thermometers overestimate the temperature. Moreover, they addressed the fact that several chlorite generations may exist in the same rock that formed over a large T range.

5.6 Origin of synchysite-(Ce)

From all Variscan granites of the Erzgebirge−Vogtland metallogenic province, the granites and aplites from Eichigt/Schönbrunn are richest in synchysite-(Ce). This REE fluorocarbonate may have originated late-magmatically from the granite and aplite melts containing LREE in excess to what could be fixed in monazite-(Ce), and/or post-magmatically from the LREE budget of monazite-(Ce) dissolved by F–CO_2-rich fluids. Our favorite hypothesis involves a secondary origin of the bulk of the synchysite-(Ce) in the studied granite/aplite, as evident for all previously reported occurrences of this species in granites of the province, such as Niederbobritzsch (Förster 2000), Markersbach (Förster 2001) und Zinnwald/Cínovec (Johan & Johan 2005, Förster et al. 2011).

However, there is some possibility that not all of the synchysite-(Ce) is secondary in origin, a hypothesis also raised for other P-poor A-tye granites (cf. Andersson & Förster 2016). Noteworthy, Synchysite-(Ce) of almost identical composition is distributed within the entire Eichigt−Schönbrunn structure and displays no correlation with the lithology of the country rock in which the granite apical intrusions are emplaced. This observation suggests that the parental magma, which may have been originally enriched in CO_2 by partial melting of CO_2-bearing lithologies, may have received its fertility to crystallize this mineral somewhere on its way from the source to the level of emplacement and subsequent separation of different magma batches. More work is needed to verify this hypothesis.

5.7 Metallogenic perspective

The Eichigt−Schönbrunn granite massif is spatially associated with minor Sn-polymetal mineralization near the town of Oelsnitz, which was previously discussed as probably being genetically related. As to the potential for Sn, unaltered samples of granites of the Erzgebirge−Vogtland metallogenic province and elsewhere, which gave rise to orthomagmatic Sn mineralization (triggered by Sn-rich residual fluids), typically bear elevated Sn concentrations exceeding 25 ppm. Accordingly, all samples studied here contain considerably less Sn (cf. Table 5) as would requiered to classify them as Sn-perspective. The same holds for samples from the neighbouring Schönbrunn apical intrusion. Alteration that the samples experienced was not that serious as the one could assume secondary element-depletion caused by overprinting as being responsible for the measured present-day Sn contents. Furthermore, Sn-mobilization from the crystal

structure of primary trioctahedral micas by external fluids could as well not account for the formation of the cassiterite-bearing veins since these minerals lack signs of complete alteration. Mobilization of Sn, W and other granite-related ore elements has been recently invoked to explain the origin of tin greisen and vein mineralization associated wuith the Zinnwald/Činovec granite in the eastern Erzgebirge/Krušné hory by Johan et al. (2012). To conclude, a genetical association of the spatially related Sn mineralization to the Eichigt-Schönbrunn granite massif could not be excluded, but is not yet substantiated by hard evidence.

5.8 Geochronological position

Bielicki & Tischendorf (1991) calculated a thorogenic Pb/Pb model age of 296 ± 3 Ma for K-feldspar from the Eichigt granite, which is little younger than the Th–U–total Pb uraninite age of 305.3 ± 3.0 Ma reported in this study. These ages imply that the magmatism at Eichigt probably occurred in the latest Carboniferous, near the Carboniferous/Permian boundary. The granite melts were generated during the same period of magmatismus, in which the nearby, chemically similar rhyolite/microgranite association at Gottesberg (304 ± 5 Ma, K–Ar on siderophyllite, Förster et al. 2007) and the more distant aluminous A-type granite from Seiffen in the eastern Erzgebirge (302 ± 4 Ma, Th–U–total Pb on monazite, Förster & Rhede 2006) formed. The emplacement of the Henneberg granite massif in Thuringia (299 ± 6 Ma, U–Pb SHRIMP on zircon, Loth et al. 1999; 300 ± 1 Ma, Re–Os on molybdenite, Hannah et al. 2007), some 45 km NW of Eichigt, occurred also during this event. The magmatic rocks from Eichigt postdate the intrusion of the large neighbouring multiphase granite massifs of Bergen, Kirchberg, and Eibenstock (cf. Fig. 1) by about 15 – 20 Ma (see Förster & Romer 2010, and Tichomirowa & Leonhardt 2010, for a compilation of references).

5.9 Sequence of rock- and mineral-forming processes

Summarizing, the following stages of formation of the Eichigt granite could be discriminated (cf. Table 4).

1. Crystallization of Qz-A_1, Kfs-A_1, Bt-A, Pl-A(?), and andalusite within a lesser felsic progenitor/forerunner magma. This probably cogenetic magma was richer in Ti and hotter than the Eichigt granite magma (see zonal and high-luminescent Qz-A_1; Fig. 11). It was also richer in Ba (see higher Ba content of Kfs-A_1; Fig. 10) and several trace elements (see paragenesis of Bt-A with accessory minerals, Fig. 4e). The lower F content of the forerunner magma triggered the formation of andalusite instead of topaz.

2. Incorporation of some early crystallized minerals from the forerunner magma as antecrysts into the Eichigt granite magma, thereby interrupting their growth connected with changed chemical composition and lower temperature of the more felsic Eichigt melt. The antecrysts reacted as follows: Qz-A_1 was rounded; newly grown quartz developed a lower-luminescent (i.e., Ti-poorer) zoning (Fig. 11). Bt-A started to equilibrate (Al, [Fe+Ti]; Fig. 5). Andalusite was replaced by topaz (Fig. 14e). Kfs-

A_1 was rounded and mantled by fine-grained, locally granophyric Kfs + Qz, with Kfs composition equaling that of Kfs-A_2 (Fig. 10), as did Qz-A_1 and the one enclave-bearing plagioclase phenocryst Pl-A(?) (Fig. 13a), implying a simultaneous growth under nonequilibrium conditions (Fenn 1986).

3. In the Eichigt granite magma now containing a small portion of the antecryst-providing forerunner melt, the true phenocrysts of Kfs-A_2, Qz-A_2, the cores of larger biotite grains (Bt-B; Fig. 4f), and, probably, the small biotite flakes in Qz started to grow in the magma chamber at the level of anatectic melting. During magma uprise and final emplacement, the matrix with Qz-B, Kfs-B, plagioclase, and Bt-C solidified. Again, granophyric and/or fine-grained rims crystallized overgrowing the true phenocrysts. Within the matrix, small granophyric isles originated. Such granophyres are typical for water-enriched, strongly undercooled magmas, which underwent isothermal decompression (Lowenstern et al. 1997). After Charoy & Raimbault (1994) and Lowenstern et al. (1997), these textures typify a shallow level of emplacement, i.e., a subvolcanic setting.

4. The final stage of the residual-melt solidification took place in a water-enriched, silica-oversaturated environment. Late-magmatic crystallization involves precipitation of the latest primary minerals, namely, large, occasionally euhedral topaz (Figs. 14c; 14d) and Na–Al-rich white mica (WM-A) hosted in feldspars, crystallized on grain boundaries, or forming the cores of inhomogeneous white-mica grains (Figs. 6d; 7). Simultaneously, replacement reactions started, in particular characterized by the intense corrosion of all earlier formed minerals by Qz-C (Fig. 13b).

5. Subsequent post-magmatic processes in the solid granite are characterized by markedly increased fluorine contents of the migrating solutions, which gave rise to the formation of the F-rich white mica WM-B (Fig. 7) crystallizing in interstices between pre-existing minerals (Figs. 6b; 6c) and the onset of replacement of biotite by chlorite. Also synchysite-(Ce) and fluorite likely crystallized at this stage. Minor cataclasis occurred locally, indicated by kinked bands in altered biotite (Fig.4a), fractures in feldspars and quartz, and the formation of Qz-D_1 and Qz-D_2 in fissures (Fig. 11).

6. At same later (hydrothermal) stage, percolation of F-poor hydrous solutions caused another event of chloritization and resulted in the crystallization of the F-free white mica WM-C, again accompanied by minor fracturing.

Acknowledgements

The authors are greatful to a team of analytical chemists at the Helmholtz Centre Potsdam German Research Center for Geosciences GFZ performing the whole-rock analyses: R. Naumann, P. Dulski, K. Hahne and G. Schettler. O. Appelt and D. Rhede assisted with the electron-microprobe analyses. A. Hendrich and M. Dziggel have drawn the figures. P. Suhr, Sächsisches Landesamt für Umwelt, Landwirtschaft and Geologie, and A. Hiller, Geological Archive of the WISMUT GmbH, are thanked for providing access to literature information.

References

Abdel-Rahman, A.-F.M. (1994): Nature of biotites from alkaline, calc-alkaline, and peraluminous magmas. − J. Petrol. **35**: 525−541.

Agangi, A., Kamenetsky, V.S., Hofmann, A., Przybyłowicz, W. & Vladykin, N.V. (2014): Crystallisation of magmatic topaz and implications for Nb−Ta−W mineralisation in F-rich silicic melts − The Ary-Bulak ongonite massif. − Lithos **202−203**: 317−330.

Alfonso, P., Melgaejo, J.C., Yusta, I. & Velasco, F. (2003): Geochemistry of feldspars and muscovite in granitic pegmatite from the Cap de Creus field, Catalonia, Spain. – Canad**.** Miner. **41**: 103−116.

Andersson, U.B. & Förster, H.-J. (2016): Magmatic evolution of the Rödö rapakivi complex (Sweden); the importance of REE-fluorocarbonates. In: 35th Int. Geol. Congress, Cape Town, South Africa, Aug. 27 − Sept. 4, Conf. Volume, pap. No. 3435.

Bailey, S.W. (1980): Summary of recommendations of AIPEA nomenclature committee on clay minerals. − Amer. Miner. **65**: 1−7.

Bailey, S.W. (1988): Chlorites: Structures and Crystal Chemistry. In: Bailey, S.W. (ed.): Hydrous Phyllosilicates (Exclusive of Micas). − Reviews in Mineralogy **19**, 347−403. Mineralogical Society of America, Chelsea/Michigan.

Barbarin, B. (1991): Enclaves of the Mesozoic calc-alkaline granitoids of the Sierra Nevada Batholith, California. In: Didier, J. & Barbarin, B. (eds.): Enclaves and Granite Petrology. – Developments in Petrology **13**, 135−153. Elsevier, Amsterdam-Oxford-New York-Tokyo.

Baumann, L., Bernstein, K.-H., Kämpf, H. & Wolf, P. (1982): Zur minerogenetischen Bedeutung von Bruchstrukturen am NW-Rand des Böhmischen Massivs (Bereich Vogtland). – Z. angew. Geol. **28,** 463−470.

Baxter, S. & Feely, M. (2002): Magma mixing and mingling textures in granitoids: examples from the Galway Granite, Connemara, Ireland. – Mineral.Petrol. **76**: 63−74.

Bayliss, P. (1975): Nomenclature of the trioctahedral chlorites. − Canad. Miner.**13:** 178−180.

Behr, H.-J. & Frentzel-Beyme, K. (1989): Permeability and paleoporosity in crystalline bedrocks of the central European basement; studies of cathodoluminescence. − In: Boden, A. & Eriksson, K.G. (eds.): Exploration of the Deep Continental Crust. Deep Drilling in Crystalline Bedrock. Vol. 2, 477−497. Berlin-Heidelberg-New York.

Bielicki, K.-H. & Tischendorf, G. (1991): Lead isotope and Pb − Pb model age determinations of ores from Central Europe and their metallogenetic interpretation. − Contrib. Miner. Petrol. **106**: 440−461.

Bourdelle, F., Parra, T., Beyssac, O., Chopin, C. & Vidal, O. (2013): Clay minerals as geo-thermometer: A comparative study based on high spatial resolution analyses of illite and chlorite in Gulf Coast sandstones (Texas, U.S.A.). − Amer. Miner. **98**: 914−926.

Bowles, J.F.W. (1990): Age dating of individual grains of uraninite in rocks from electron microprobe analysis. – Chem. Geol. **83**: 47–53,

Breiter, K. (2002): From explosive breccia to unidirectional solidification textures: magmatic evolution of a phosphorus- and fluorine-rich granite system (Podlesí, Krušné hory Mts., Czech Republic). – Bull. Czech Geol. Survey **77**: 67−92.

Breiter, K., Gardenová, N., Vaculovič, T & Kanický, V. (2013): Topaz as important host for Ge in granites and greisens. − Miner. Mag. **77**: 403−417.

Breiter, K. & Kronz, A. (2004): Phosphorus-rich topaz from fractionated granites (Podlesí, Czech Republic). – Mineral.. Petrol. **81**: 235−247.

Cathelineau, M. (1988): Cation site occupancy in chlorites and illites as a function of temperature. − Clay Minerals **23:** 471−485.

Cathelineau, M. & Nieva, D. (1985): A chlorite solid solution geothermometer. The Los Azufres (Mexico) geothermal system. − Contrib. Miner. Petrol. **91:** 235−244.

Černý, P. & Burt, D.M. (1984): Paragenesis, crystallochemical characteristics, and geochemical evolution of micas in granitic pegmatites. – In: Bailey, S.W. (ed.): Micas. Reviews in Mineralogy **13**: 257−297; Chelsea / Michigan.

Charlier, B.L.A., Wilson, C.J.N., Lowenstern, J.B., Blake, S., Van Calsteren, P.W. & Davidson, J.P. (2005): Magma generation at a large, hyperactive silicic volcano (Taupo, New Zealand) revealed by U-Th and U-Pb systematics in zircons. − J. Petrol. **27**: 3−32.

Charoy, B. (1986): The genesis of the Cornubian batholith (south-west England): the example of the Carnmenellis pluton. – J. Petrol. **27**: 571–604.

Charoy, B. & Raimbault, L. (1994): Zr-, Th-, and REE-rich biotite differentiates in the A-type granite pluton of Suzshou (eastern China): the key role of fluorine. – J. Petrol. **35**: 919−962.

Clarke, D.B., Dorais, M., Barbarin, B., Barker, D., Cesare, B., Clarke, G., El Baghdadi, M., Erdmann, S., Förster, H.-J., Gaeta, M., Gottesmann, B., Jamieson, R.A., Kontak, D., Koller, F., Leal Gomes, C., London, D., Morgan VI, G.B., Neves, L.J.P.F., Pattison, D.R.M., Pereira, A.J.S.C., Pichavant, M., Rapela, C.W., Renno, A.D., Richards, S., M., Rottura, A., Saavedra, J., Sial, A.N., Toselli, A.J., Ugidos, J.M., Uher, P., Villaseca, C., Visonà, D., Whitney, D.L., Williamson, B. & Woodard, H.H. (2005): Occurrence and origin of andalusite in peraluminous felsic igneous rocks. – J. Petrol. **46**: 441−472.

Clarke, D.B., Wunder, B., Förster, H.-J., Rhede, D. & Hahn, A. (2009): Experimental investigation of near-liquidus andalusite-topaz relations in synthetic peraluminous haplogranites at 200 MPa. – Miner. Mag. **73**: 997−1007.

Cox, R.A., Dempster, T.J., Bell, B.R. & Rogers, G. (1996): Crystallization of the Shap granite: evidence from zoned K-feldspar megacrysts. – J. Geol. Soc. **153**: 625−635.

Dahlquist, J.A., Alasino, P.H., Eby, G.N., Galindo, C. & Casquet, C. (2010): Fault controlled Carboniferous A-type magmatism in the proto-Andean foreland (Sierras Pampeanas, Argentina): Geochemical constraints and petrogenesis. − Lithos **115**: 65−81.

Dahlquist, J.A., Rapela, C.W. & Baldo, E.G. (2005): Petrogenesis of cordierite-bearing S-type granitoids in Sierra de Chepes, Famatinian orogen, Argentina. – J. South Amer. Earth Sci. **20**: 231−151.

Davidson, J., Morgan D.J., Charlier, B.L.A., Harlou, R. & Hora, J.M. (2007): Microsampling and isotopic analysis of igneous rocks: Implications for the study of magmatic systems. – Ann. Rev.EarthPlanet. Sci. **35**: 273−311.

De Caritat, P., Hutcheon, I. & Walshe, J.L. (1993): Chlorite geothermometry: a review. − Clays Clay Minerals **41**: 219−239.

Deer, W.A., Howie, R.A. & Zussman, J. (2003): Rock-Forming Minerals. Sheet Silicates. Micas. − Vol. 3A, 2nd edition. By FLEET, M.E., The Geological Society of London, London.

Dempster, T.J., Tanner, P.W.G. & Ainsworth, P. (1994): Chemical zoning of white micas: A record of fluid infiltration in the Oughterard granite, western Ireland. – Amer. Miner. **79**: 536−544.

D'Lemos, R.S., Kearsley, A.T., Pembroke, J.W., Watt, G.R. & Wright, P. (1997): Complex quartz growth histories in granite revealed by scanning cathodoluminescence techniques. − Geol. Mag. **134**: 459−552.

Du Bray, E.A. (1994): Compositions of micas in peraluminous granitoids of the eastern Arabian Shield. – Contrib. Miner. Petrol. **116**: 381−397.

Dudek, A. (1987): Geology and tectonic pattern of theWestern Bohemia seismic area. − In: Prochazkova, D. (ed.): Earthquake Swarm 1985/86 in Western Bohemia. Proceedings of workshop in Marianske Lazne, Dec. 1−5, 1986, 34−37: Czechoslovak Academy of Sciences, Geophysical Institute Praha, Praha.

Dulski, P. (2001): Reference materials for geochemical studies: new analytical data by ICP-MS and critical discussion of reference values. – Geostandards Newsletter **25**: 87–125.

Fenn, P.M. (1986): On the origin of graphic granite. – Amer. Miner. **71**: 325−330.

Förster, H.-J. (1998a): The chemical composition of REE–Y–Th–U rich accessory minerals in peraluminous granites of the Erzgebirge–Fichtelgebirge region, Germany, part I: The monazite-(Ce) – brabantite solid solution series. – Amer. Miner. **83**: 259–282.

Förster, H.-J. (1998b): The chemical composition of REE–Y–Th–U-rich accessory minerals in peraluminous granites of the Erzgebirge–Fichtelgebirge region, Germany, part II: Xenotime. – Amer. Miner. **83**: 1302–1315.

Förster, H.-J. (1999): The chemical composition of uraninite in Variscan granites of the Erzgebirge, Germany. − Miner. Mag. **63:** 239−252.

Förster, H.-J. (2000): Cerite-(Ce) and thorian synchysite-(Ce) from the Niederbobritzsch granite (Erzgebirge, Germany): implications for the differential mobility of Th and the LREE during alteration. − Canad. Mineral. **38:** 67−79.

Förster, H.-J. (2001): Synchysite-(Y) − synchysite-(Ce) solid solutions from Markersbach, Erzgebirge, Germany: REE and Th mobility during high-T alteration of highly fractionated aluminous A-type granites. − Mineral. Petrol. **72:** 259−280.

Förster, H.-J. & Tischendorf, G. (1996): Compositional heterogeneity of silicic magmatic rocks from the German Variscides. – Z. geol. Wiss., 24, 3/4, 467–482.

Förster, H.-J., Gottesmann, B., Tischendorf, G., Siebel, W., Rhede, D., Seltmann, R. & Wasternack, J. (2007): Permocarboniferous subvolcanic rhyolite dikes in the western Erzgebirge/Vogtland, Germany: a record of source heterogeneity of post-collisional felsic magmatism. – N. Jb. Miner. Abh. **183**: 123–147.

Förster, H.-J. & Rhede, D. (2006): The Ba–Ta-rich granite of Seiffen (eastern Erzgebirge, Germany): accessory-mineral chemistry, composition, and age of a late-Variscan Li–F granite of A-type affinity. – N. Jb. Miner. Abh. **182**: 307–321.

Förster, H.-J., Rhede, D. & Hecht, L. (2008): Chemical composition of radioactive accessory minerals: implications to the evolution, alteration, age, and uranium fertility of the Fichtelgebirge granites (NE Bavaria, Germany) – N. Jb. Miner. Abh. **185**: 161–182.

Förster, H.-J. & Romer, R.L. (2010): Carboniferous magmatism. In: LINNEMANN, U., KRONER, U., & ROMER, R.L. (eds.): From Cadomian Active Margin to the Core of the Variscan Orogen: The pre-Mesozoic Geology of Saxo-Thuringia (NE Bohemian Massif). – E. Schweizerbart`sche Verlagsbuchhandlung, Stuttgart, 287−308.

Förster, H.-J., Seltmann, R. & Tischendorf, G. (1995): High-fluorine, low-phosphorus A-type (post-collision) silicic magmatism in the Erzgebirge. – In: 2nd Symposium on Permocarboniferous Igneous Rocks. Potsdam, October 27-29, Ext. Abstr., Terra Nostra **7**: 32−35.

Förster, H.-J., Tischendorf, G., Seltmann, R. & Gottesmann, B. (1998): Die variszischen Granite des Erzgebirges: neue Aspekte aus stofflicher Sicht. – Z. geol. Wiss. **26**: 31–60.

Förster, H.-J., Tischendorf, G., Trumbull, R.B. & Gottesmann, B. (1999): Late-collisional granites in the Variscan Erzgebirge, Germany. – J. Petrol. **40**: 1613−1645.

Förster, H.-J., Ondrejka, M. & Uher, P. (2011): Mineralogical responses to subsolidus alteration of granitic rocks by oxydizing As-bearing fluids: REE arsenates and As-rich silicates from the Zinnwald granite, Eastern Erzgebirge. − Canad. Mineral. **49**: 913−930.

Foster, M.D. (1960): Interpretation of the composition of trioctahedral micas. − U.S. Geol. Survey, Prof. Pap. **354-B**, 11−49.

Frimmel, H.E. ((1997): Chlorite thermometry in the Witwatersrand Basin: Constraints on the Paleoproterozoic geotherm in the Kaapvaal Craton, South Africa. − J. Geol. **105:** 601−615.

Gagnevin, D., Daly, J.S., Poli, G. & Morgan, D. (2005): Microchemical and Sr isotopic investigation of zoned K-feldspar megacrysts: Insights into the petrogenesis of a granitic system and disequilibrium crystal growth. – J. Petrol. **46**: 1689−1724.

Gioncada, A., Orlandi, P., Vezzoli, L., Omarini, R.H., Mazzuoli, R., Lopez-Azarevich, V., Sureda, R., Azarevich, M., Acocella, V. & Ruch, J. (2014): Topaz magmatic crystallization in rhyolites of the Central Andes (Chivinar volcanic complex, NW Argentina): Constraints from texture, mineralogy and rock chemistry. − Lithos **184−187**: 62−73.

Gomes, M.E.P., Neiva, A.M.R. (2000): Chemical zoning of muscovite from the Ervedosa granite, northern Portugal. – Miner. Mag. **64**: 347−358.

Gottesmann, B., Seltmann, R. & Förster, H.-J. (1995): Felsic subvolcanic intrusions within the Eibenstock granite pluton (Saxony, Germany): The Gottesberg volcano-plutonic system. − Terra Nostra **7**, 49−53.

Gottesmann, B., Förster, H.-J., Tischendorf, G. & Seltmann, R. (1996): Geochemistry and mica composition of the Gottesberg subvolcanic A-type suite (Saxony, Germany). – V.M. Goldschmidt Conference, Heidelberg/Germany, March 31–April 4, 1996. Journal of Conference Abstracts Vol.1 (1), 208.

Grogan, S.E. & Reavy, R.J. (2002): Disequilibrium textures in the Leinster Granite Complex, SE Ireland: evidence for acid-acid magma mixing. – Miner. Mag. **66**: 929−939.

Grosse, S., Oelsner, C. & Bremer, H. (1961): Über die gravimetrische Vermessung des Vogtlandes und des Erzgebirges. – Z,angew, Geol, **7**: 357−362.

Hannah, J.L., Stein, H.J., Wieser, M.E., de Laeter, J.R. & Varner, M.D. (2007): Molybdenum isotope variations in molybdenite: Vapor transport and Rayleigh fractionation of Mo. – Geology **35:** 703-706.

Herrmann, G. (1967): Die Granite des Westerzgebirges und des Vogtlandes und ihre Beziehungen zu granitischen Gesteinen der benachbarten Räume. – Dissertation Bergakademie Freiberg. Textband 205 S., Anlagenband 356 S.

Hibbard, M.J. (1991): Textural anatomy of twelve magma-mixed granitoid systems. - In: DIDIER, J. & BARBARIN, B. (eds.): Enclaves and Granite Petrology. – Developments in Petrology **13**, 431−444. Elsevier, Amsterdam-Oxford-New York-Tokyo.

Hillier, S. & Velde, B. (1991): Octahedral occupancy and the chemical composition of diagenetic (low-temperature) chlorites. − Clay Minerals **26:** 149−168.

Huang, R. & Audétat, A. (2012): The titanium-in-quartz (TitaniQ) thermobarometer: A critical examination and re-calibration. − Geochim. Cosmochim. Acta **84:** 75−89.

Jiang, W.-T., Peacor, D.R. & Buseck, P.R. (1994): Chlorite geothermometry? – Contamination and apparent octahedral vacancies. − Clays Clay Minerals **42**: 593−605.

Johan, Z. & Johan, V. (2005): Accessory minerals of the Cínovec (Zinnwald) granite cupola, Czech Republic: indicators of petrogenetic evolution. − Mineral, Petrol. **83:** 113−150.

Johan, Z., Stmad, L., Johan, V. (2012): Evolution of the Cínovec (Zinnwald) granite cupola, Czech republic: Composition of feldspars and micas, a clue to the origin of W,Sn mineralization. – Canad. Mineral., 40, 1131−1148.

Jolliff, B.L., Papike, J.J. & Shearer, C.K. (1987): Fractionation trends in mica and tourmaline as indicators of pegmatite internal evolution: Bob Ingerson pegmatite, Black Hills, South Dakota. – Geochim. Cosmochim. Acta **51**: 519−534.

Jowett, E.C. (1991): Fitting iron and magnesium into the hydrothermal chlorite geothermometer. − Program with Abstracts of GAC, MAC, SEG Joint Annual Meeting, Toronto 1991.

Kämpf, H., Strauch, G., Klemm, W., Bielicki, K.-H., Geißler, M., Haase, G., Köhler, M., Meixner, A., Mingram, B., Thomas, R., & Vogler, P. (1991a): Hydrothermale Spatmineralisation Erzgebirge. − Unpublished Report, Zentralinstitut für Physik der Erde Potsdam, 70 p.

Kämpf, H., Thomas, R., Kuschka, E. & Klemm, W. (1991b): Die Quarz-Kassiterit-Gänge im Endo- und Exokontakt des verdeckten Granitmassives von Eichigt-Schönbrunn. – Geoprofil, Freiberg **3**, 55−62.

Kempe, U. (2003): Precise electron microprobe age determination in unaltered uraninite: consequences on the intrusion age and the metallogenetic significance of the Kirchberg granite (Erzgebirge, Germany). – Contrib. Miner. Petrol. **145**: 107–11.

Konings, R.J.M., Boland, J.N., Vriend, S.P. & Jansen, J.B.H. (1988): Chemistry of biotites and muscovites in the Abas granite, northern Portugal. – Amer. Miner. **73**: 754−765.

Kontak, D.J. (1991): The East Kemptville topaz-muscovite leucogranite, Nova Scotia; II, Mineral chemistry. – Canad. Miner. **29**: 37−60.

Kozlowski, A. (1981): Melt inclusions in pyroclastic quartz from the Carboniferous deposits of the Holy Cross Mts. and the problem of magmatic corrosion. − Acta Geol. Polonica **31**: 273−283.

Kranidiotis, P. & MacLean, W.H. (1987): Systematics of chlorite alteration at the Phelps Dodge massive sulphide deposit, Matagami, Quebec. − Econ. Geol. **82:** 1898−1911.

Kuschka, E. & Hahn, W. (1996): Flußspatlagerstätten des Südwestvogtlandes: Schönbrunn, Bösenbrunn, Wiedersberg. − Bergbau in Sachsen **2**: 1−283.

Laemmlein, G. (1930): Korrosion und Regeneration der Porphyr-Quarze. – Z. Krist. **75**: 109−127.

Le Bas, M.J. & Streckeisen, A.L. (1991): The IUGS systematics of igneous rocks. – J. Geol. Soc. London**146**: 825−833.

Loth, G., Höll, R., Ritter-Höll, A., Bartzsch, K. and Kennedy, A. (1999): U-PB SHRIMP-Alter von Zirkonen aus dem Biotit-Granit der Henneberg-Intrusion (Thüringen). – Beiträge zur Geologie von Thüringen, Neue Folge 6: 209-215.

Lowenstern, J.B. (1995): Applications of silicate-melt inclusions to the study of magmatic volatiles. In: Thompson, J.H.F. (ed.): Magmas, Fluids and Ore Deposits. − Mineral. Assoc. Canada Short Course **23**: 71−99.

Lowenstern, J.B., Clynne M.A. & Bullen, T.D. (1997) Comagmatic A-Type granophyre and rhyolite from the Alid volcanic center, Eritrea, Northeast Africa. − J. Petrol. **38**: 1707−1721.

Ludwig, K.R. (1999): Users manual for ISOPLOT/EX, version 2. A geochronological toolkit for Microsoft Exel. – Berkeley Geochronological Center, Spec. Publ. 1a, 43 pp.

Miller, C.F., Stoddard, E.F., Bradfish, L.J. & Dollase, W.A. (1981): Composition of plutonic muscovite: genetic implications. – Canad. Miner. **19**: 25−34.

Monier, G., Mergoil-Daniel, J. & Labernardière, H. (1984): Générations successives de muscovites et feldspaths potassiques dans les leucogranites du massif de Millevaches (Massif Central français). − Bull. Minéral. **107**: 55−68.

Müller, A., Kronz, A. & Breiter, K. (2002a): Trace elements and growth patterns in quartz: a fingerprint of the evolution of the subvolcanic Podlesí Granite System (Krušne Hory, Czech Republic). − Bull. Czech Geol. Survey **77**/2: 135−145.

Müller, A., Lennox, P. & Trzebski, R. (2002b): Cathodoluminescence and micro-structural evidence for crystallisation and deformation processes of granites in the Eastern Lachlan Fold Belt (SE Australia). − Contrib. Miner. Petrol. **143**: 510−524.

Müller, A., Seltmann, R. & Behr, H.-J. (2000): Application of cathodoluminescence to magmatic quartz in a tin granite − case study from the Schellerhau Granite Complex, Eastern Erzgebirge, Germany. − Miner. Deposita **35**: 169–189.

Müller, A., Rene, M., Behr, H.-J. & Kronz, A. (2003): Trace elements and cathodoluminescence of igneous quartz in topaz granites from the Hub Stock (Slavkovský Les Mts., Czech Republic). − Mineral. Petrol. **79**: 167−191.

Müller, A., Breiter, K., Seltmann, R. & Pécskay, Z. (2005): Quartz and feldspar zoning in the eastern Erzgebirge volcano-plutonic complex (Germany, Czech Republic): evidence of multiple magma mixing. − Lithos **80**: 201−227.

Müller, A., Behr, H.-J., Van den Kerkhof, A.M., Kronz, A. & Koch-Müller, M. (2010): The evolution of late-Hercynian granites and rhyolites documented by quartz − a review. − Earth and Environmental Science Transactions of the Royal Society of Edinburgh **100**: 185−204.

Nachit, H., Razifimahefa, N., Stussi, J.M. & Carron, J.P. (1985): Composition chimique des biotites et typologie magmatique des granitoides. – C. R. Acad. Sci. Paris **301**, 813−818.

Plessen, H.-G., Rothe, H., Zimmer, M. & Erzinger, J. – In: Govindaraju, K., Potts, P. J., Webb, P. C. & Watson, J. S. (1994): Report on Whin Sill Dolerite WS-E from England and Pitscurrie Microgabbro PM-S from Scotland: assessment by one hundred and four international laboratories. – Geostandards Newsletter **18:** 211–300.

Quellmalz, W. (1959): Lagerstättengenetische und tektonische Untersuchungen der an die Schönbrunner Spalte geknüpften hydrothermalen Lagerstätten des Vogtlandes. – Jb. Staatl. Mus. Mineral. Geol. Dresden **1959**, 1−38.

Rieder, M., Cavazzini, G., D'yakonov, Yu.S., Frank-Kamenetskii, V.A., Gottardi, G., Guggenheim, S., Koval', P.V., Müller, G., Neiva, A.M.R., Radoslovich, E.W., Robert, J.-L., Sassi, F.P., Takeda, H., Weiss, Z. & Wones, D.R. (1998): Nomenclature of the micas. – Canad. Miner. **36**: 905−912.

Romer, R.L., Thomas, R., Stein, H.J. & Rhede, D. (2007): Dating multiply overprinted Sn-mineralized granites – examples from the Erzgebirge, Germany. – Miner. Deposita **42**: 337–359.

Ruggieri, G., Petrone, C.M., Gianelli, G., Arias, A. & Henriquez, E. (2006): Hydrothermal alteration in the Berlin geothermal field (El Salvador): new data and discussionon the natural state of the system. − Periodico di Mineralogia **75:** 293−312.

Schützel, H. & Hösel, G. (1962): Eine neue Mineralquelle im südwestlichen Vogtland und Bemerkungen zum Granitmassiv von Eichigt-Schönbrunn. – Z.angew. Geol. **8**: 404−408.

Shannon, J.R., Walker, B.M., Carten, R.B. & Geraghty, E.P. (1982): Unidirectional solidification textures and their significance in determining relative ages of intrusions at the Henderson mine, Colorado. – Geology, **10**: 293−297.

Słaby, E., Galbarczyk-Gąsiorowska, L., Seltmann, R. & Müller, A. (2007a): Alkali feldspar megacryst growth: Geochemical modelling. – Mineral. Petrol. **89**: 1−29.

Słaby, E., Seltmann, R., Kober, B., Müller, A., Galbarczyk-Gąsiorowska, L. & Jeffries, T. (2007b): LREE distribution patterns in zoned alkali feldspar megacrysts from the Karkonosze pluton, Bohemian Massif – implications for parental magma composition. – Miner. Mag. **71**: 155−178.

Speer, J.A. (1984): Micas in igneous rocks. – In: S.W.BAILEY (ed.): Micas. Reviews in Mineralogy **13**: 299−356; Chelsea / Michigan.

Sprunt, E.S. & Nur, A. (1979): Microcracking and healing in granites: New evidence from cathodoluminescence. − Science **205**: 495−497.

Steiger, R.H. & Jäger, E. (1977): Subcommission on geochronology: convention on the use of decay constants in geo- and cosmochronology. – Earth Planet. Sci. Lett. **36**: 359–362.

Thomas, R. (1982): Ergebnisse der thermobarogeochemischen Untersuchungen an Flüssigkeitseinschlüssen in Mineralen der postmagmatischen Zinn-Wolfram-Mineralisation des Erzgebirges. – Freiberger Forschungshefte **C 370**: 85 pp.; Leipzig.

Tichomirowa, M. & Leonhardt, D. (2010): New age determinations (Pb/Pb zircon evaporation, Rb/Sr) on the granites from Aue-Schwarzenberg and Eibenstock, Western Erzgebirge, Germany. – Z. geol. Wiss. **38**: 99−123.

Tischendorf, G., Förster, H.-J. & Gottesmann, B. (1999a): The correlation between lithium and magnesium in trioctahedral micas: Improved equations for Li_2O estimation from MgO data. – Miner. Mag. **63**: 57−74.

Tischendorf, G., Förster, H.-J. & Gottesmann, B. (1999b): Tri- und dioktaedrische Glimmer in Granitoiden aus dem Osten Deutschlands – Historie ihrer Untersuchung und neue Forschungsergebnisse. – Z. geol. Wiss. **27**: 427−442.

Tischendorf, G., Förster, H.-J., Gottesmann, B. & Rieder, M. (2007): True and brittle micas: Composition and solid-solution series. – Miner. Mag. **71**: 285−320.

Tischendorf, G., Rieder, M., Förster, H.-J., Gottesmann, B. & Guidotti, C.V. (2004): A new graphical presentation and subdivision of potassium micas. - Miner. Mag. **68**: 649−667.

Valley, J.W. & Graham, C.M. (1996): Ion microprobe analysis of oxygen isotope ratios in quartz from Skye granite: healed micro-cracks, fluid flow, and hydrothermal exchange. − Contrib. Miner. Petrol. **124**: 225−234.

Van den Kerkhof, A.M. & Hein, U. (2001): Fluid inclusion petrography. − Lithos **55**: 27−47.

Vernon, R.H. (1990): Crystallization and hybridism in microgranitoid enclave magmas: Microstructural evidence. – J. Geophys. Res. **95**/B 11: 17849−17859.

Vollbrecht, A., Olesen, N.O., Schmidt, N.H. & Weber, K. (1994): Crystallographic microcrack orientation in quartz from a granite – a combined ECP/U stage study. − In: Bunge, H.J., Siegesmund, S., Skrotzki, W. & Weber, K. (eds.): Textures of Geological Materials. - Oberursel: DGM Informationsgesellschaft Verlag.

Vollbrecht, A., Rust, S. & Weber, K. (1991): Development of microcracks in granites during cooling and uplift: examples from the Hercynian basement in NE Bavaria, Germany. − J. Struct. Geol. **13**: 787−799.

Wark, D.A. & Watson, E.B. (2006): TitaniQ: a titanium-in-quartz geothermometer. − Contrib. Miner. Petrol. **152**: 743−754.

Wark, D.A., Hildreth, W., Spear, F.S., Cherniak D.J. & Watson E.B. (2007): Pre-eruption recharge of the Bishop magma system. − Geology **35**: 235−238.

Weise, R. (1929): Erläuterungen zur Geologischen Karte von Sachsen im Maßstab 1 : 25000. Blatt Adorf, Nr. 151. – 2. Auflage, Leipzig. 1. Auflage: R. BECK 1884.

Weise, S.M., Bräuer, K., Kämpf, H., Strauch, G. & Koch, U.(2001): Transport of mantle volatiles through the crust traced by seismically released fluids: a natural experiment in the earthquake swarm area Vogtland/NW Bohemia, Central Europe. − Tectonophysics **336:** 137−150.

Whitney, D.L. & Evans, B.W. (2010): Abbreviations for names and rock-forming minerals. – Amer. Miner. **95**: 185−187.

Wiebe, R.A., Wark, D.A. & Hawkins, P.D. (2007): Insights from quartz cathodoluminescence zoning into crystallization of the Vinalhaven granite, coastal Maine. − Contrib. Miner. Petrol. **154**: 439−453.

Wunder, B., Andrut, M. & Wirth, R. (1999): High-pressure synthesis and properties of OH-rich topaz. – Eur. J. Miner. **11**: 803−813.

Xie, Xiaogang & Byerly, G.R. & Ferrell, R.E. Jr. (1997): IIb trioctahedral chlorite from the Barberton greenstone belt: crystal structure and rock composition constraints with implications to geothermometry. − Contrib. Miner. Petrol. **126**: 275−291.

Zane, A., Sassi, R. & Guidotti, C. (1998): New data on metamorphic chlorite as a petrogenetic indicator mineral, with special regard to greenschist-facies rocks. − Canad. Miner. **36**: 713−726.

Zang, W. & Fyfe, W.S. (1995): Chloritization of the hydrothermally altered bedrock at the Igarapé Bahia gold deposit, Carajás, Brazil. − Miner. Deposita **30**: 30−38.

Zaraisky, G.P., Aksyuk, A.M., Devyatova, V.N., Udoratina, O.V. & Chevychelov, V.Yu. (2009): The Zr/Hf ratio as a fractionation indicator of rare-metal granites. – Petrology **17**: 25–45.

Zhao, K.-D., Jiang, S.-Y. & Wang, R.-C. (2005): Mineral chemistry of the Qitianling granitoid and the Furong tin ore deposit in Hunan Province, South China: implications for the genesis of granite and related tin mineralization. − Eur. J. Miner. **17**: 635−648.

Zimák, J. (1999): Application of chlorite compositional geothermometres in hydrothermal veins in the Variscan flysch sequences of the Nízký Jeseník Upland, to Alpine-type veins in the Sobotín region, and to the paragenesis with “strigovite” from Žulová massif and Strzegom-Sobótka massif. − Acta Universitatis Palackianae Olomucensis, Facultas Rerum Naturalium, Geologica **36**: 69−74.